



Warsaw University  
of Technology

# Preliminary hydrological polar motion excitation estimates from the GRACE Follow-On mission

Justyna Śliwińska<sup>1</sup>, Małgorzata Wińska<sup>2</sup>, Jolanta Nastula<sup>1</sup>

<sup>1</sup>Space Research Centre, Polish Academy of Sciences, Warsaw, Poland

<sup>2</sup>Institute of Roads and Bridges, Warsaw University of Technology, Warsaw, Poland

# Abstract

Over almost 20 last years, observations from the Gravity Recovery and Climate Experiment (GRACE) mission have become invaluable as means to examine Earth global mass change. Since 2002, the relative along track motions between two identical satellites have been used to derive Earth's time variable gravity field. The great success and scientific sound of the mission, which ended in 2017, contributed to the launch of its successor, GRACE Follow-On (GFO) in May 2018. Until now, monthly time series of GFO-based geopotential models have been made available to the users by official GRACE data centers at Center for Space Research (CSR), Jet Propulsion Laboratory (JPL) and GeoForschungsZentrum (GFZ). This data enables the continuation of many researches which started with the beginning of the GRACE mission. Such applications included monitoring of land water storage changes, drought event identification, flood prediction, ice mass loss detection, groundwater level change analysis, and more.

In geodesy, a crucial application of GRACE/GFO mission observations is the study of polar motion (PM) changes due to mass redistribution of the Earth's surficial fluids (atmosphere, ocean, land hydrosphere). PM represents two out of five Earth Orientation Parameters (EOP), that describe the rotation of our Planet and link the terrestrial reference frame with the corresponding celestial reference frame. The use of  $C_{21}$ ,  $S_{21}$  coefficients of GRACE/GFO-based geopotential models is a common method for determining polar motion excitation.

In this study, we present the first estimates of hydrological polar motion excitation functions (Hydrological Angular Momentum, HAM) computed from GFO data which were provided by CSR, JPL and GFZ teams. The HAM are calculated using (1)  $C_{21}$ ,  $S_{21}$  coefficients of geopotential (GFO Level-2 data) as well as (2) gridded terrestrial water storage (TWS) anomalies (GFO Level-3 data). We compare and evaluate the two methods of HAM estimation and examine the compatibility between CSR, JPL and GFZ solutions. We also validate different HAM estimations using precise geodetic measurements of the pole coordinates.

Our analyses show that the highest internal agreement between different GFO solutions can be obtained when comparing CSR and JPL. Notably, GFZ estimates differ slightly from the other GFO models. The highest agreement between different GFO-based HAM, and between GFO-based HAM and reference data is obtained when GFO Level-3 data are used. We also demonstrate that the current accuracy of HAM from GRACE Follow-On mission meets the expectations and is comparable with the accuracy of HAM from GRACE Release-6 (RL06) data.

# Plan of presentation

1. Introduction
2. Motivation and objectives
3. Data and methods
4. Results
  - Internal agreement between GRACE– and GFO–based hydrological polar motion excitation estimates
  - External validation of GRACE– and GFO–based hydrological polar motion excitation estimates
  - Comparison between  $C_{21}$ ,  $S_{21}$ –based, TWS–based and mascon-based HAM
5. Conclusions

# Introduction

# Introduction

## Polar motion variations due to mass redistribution

- The Earth's gravity field varies in space and time due to disturbances in mass redistribution of Earth's surficial fluids, which include the atmosphere, oceans, and the land hydrosphere. These variations cause changes in Earth orientation parameters (EOPs), which describe the rotation of our planet. These parameters are: precession/nutation, polar motion (PM) and length-of-day (LOD) variations. EOPs are needed for e.g. precise positioning and navigation at the Earth's surface, tracking and navigating interplanetary spaceflight missions, pointing of astronomic instruments or communication with deep space objects. Therefore, they should be determined with highest possible accuracy.
- As one of the EOPs, PM is affected by a wide range of processes with different temporal variability ranging from several days to many decades. Such disturbances include not only the continuously changing mass distribution in the Earth's surficial fluids, but also the gravitational influence of celestial bodies, the effects of core–mantle coupling, as well as groundwater depletion and ice mass loss resulting from recent climate changes.
- It is commonly known that for time scales of a few years or less, the main contributors to variation in Earth's rotation are angular momentum changes of the solid Earth caused by mass redistribution in the Earth's surficial fluids. The excitation of PM due to changes in mass redistribution of atmosphere, ocean and land hydrosphere can be represented with effective angular momentum (EAM) functions: atmospheric, oceanic and hydrological (called atmospheric angular momentum AAM, oceanic angular momentum OAM, hydrological angular momentum HAM, respectively).

# Introduction

## Polar motion excitation representation

- The contribution of geophysical phenomena to the PM disturbance is usually examined by analyzing the **geophysical excitation**, which is a sum of atmospheric, oceanic and hydrological impacts:

$$\text{Geophysical Excitation} = \text{AAM} + \text{OAM} + \text{HAM}$$

- However, other geophysical effects, which are hard to measure, also contribute to this excitation (for example impact of cryosphere, earthquakes or core-mantle coupling).
- From geodetic point of view, it is possible to measure the total PM resulting from external phenomena. Modern space geodesy techniques, such as GNSS (Global Navigation Satellite Systems), SLR (Satellite Laser Ranging), and VLBI (Very Long Baseline Interferometry), provide precise observations of the pole coordinates. The current accuracy of measured EOPs is around 0.05 mas (*miliarcseconds*), which corresponds to 1.5 mm on the Earth's surface.
- So-called **geodetic excitation** of PM (or geodetic angular momentum, GAM) describes the total variation of PM which is an effect of all external impacts. GAM can be obtained from observed coordinates (x, y) of the pole by solving Liouville's equation with free Chandler wobble taken into account.

# Introduction

## Polar motion excitation representation

- If all geophysical phenomena were taken into account in determining geophysical excitation of PM, and no measurement errors would be associated with geodetic observations, the **geophysical and geodetic excitation would be equal**. However, this does not occur because of measurements errors, errors of geophysical models and omission of some geophysical effects which, for now, are hard to detect or measure (see Figs. 1 and 2).

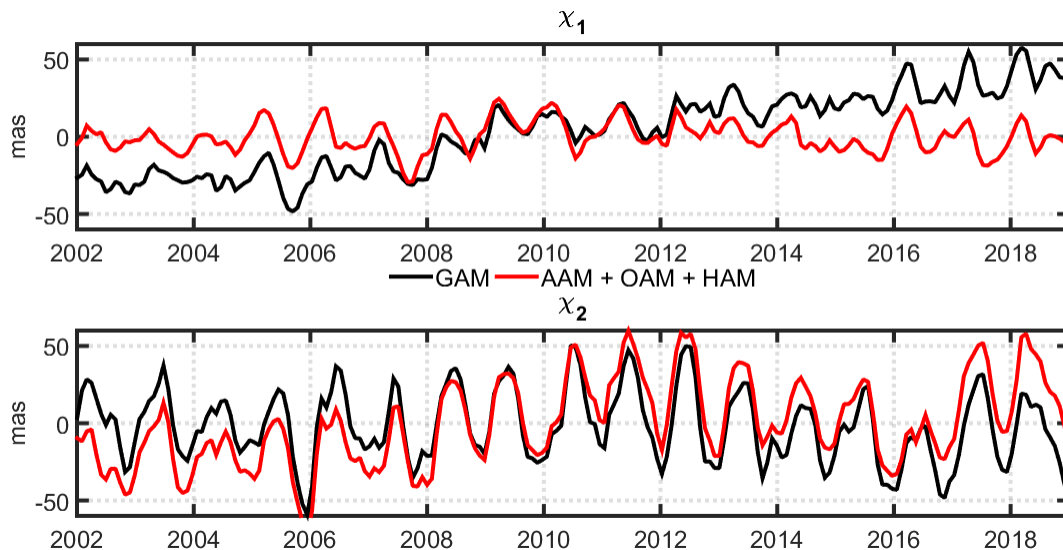


**Fig. 1.** Time series of  $\chi_1$  and  $\chi_2$  components of geodetic (GAM) and geophysical (AAM+OAM+HAM) excitation of PM. Each time series was filtered using Gaussian filter with FWHM equal to 60 days

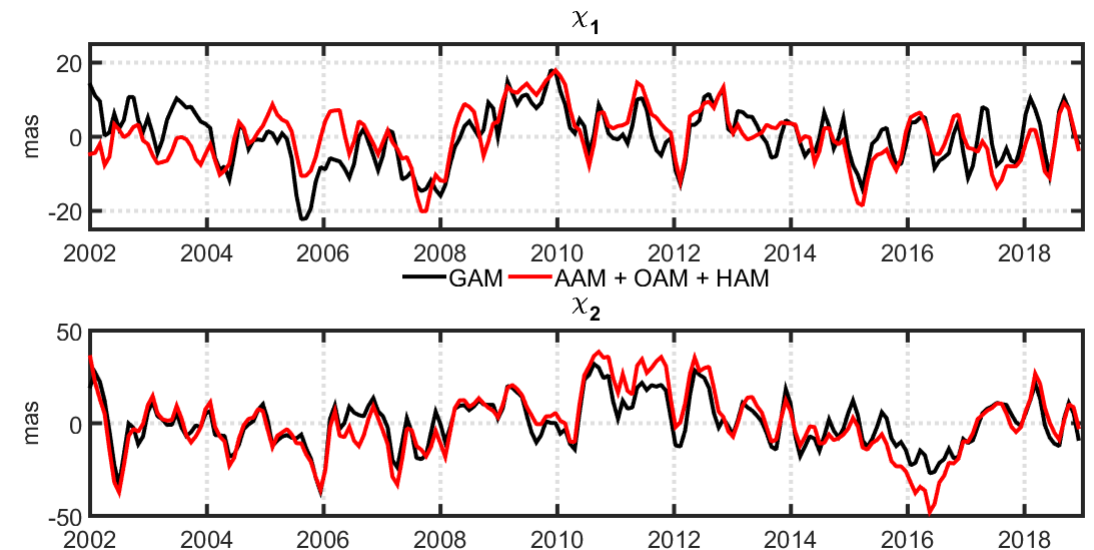


**Fig. 2.** Time series of  $\chi_1$  and  $\chi_2$  components of geodetic (GAM) and geophysical (AAM+OAM+HAM) excitation of PM after removing seasonal variations

# Introduction

## Polar motion excitation representation

- Two equatorial components of excitation function of the Earth rotation,  $\chi_1$  and  $\chi_2$ , are commonly used to describe PM excitation.  $\chi_1$  is oriented towards the Greenwich Meridian while  $\chi_2$  is oriented towards 90°E meridian. Alternatively, the complex form ( $\chi_1 + i\chi_2$ ) can be used.
- The spatial distribution of main continents and oceans causes that  $\chi_2$  is more closely related to the mass redistribution on land of the Northern Hemisphere, while  $\chi_1$  is more sensitive to mass changes over Greenland Ice Sheet and oceans.
- The axial component of Earth rotation ( $\chi_3$ ) is associated with length-of-day (LOD) variations (not considered in this study).

# Introduction

## Atmospheric, oceanic and hydrological excitation estimates

- AAM describes the impact of atmospheric pressure (mass term of AAM) and wind speed (motion term of AAM) on PM excitation, OAM is related to PM excitation due to ocean bottom pressure (mass term of OAM) and ocean currents (motion term of OAM), and HAM represents the impact of changes in continental water storage on PM variations. Such geophysical excitations of PM are determined from geophysical models of atmosphere, ocean and land hydrosphere (see Figs. 3 and 4).

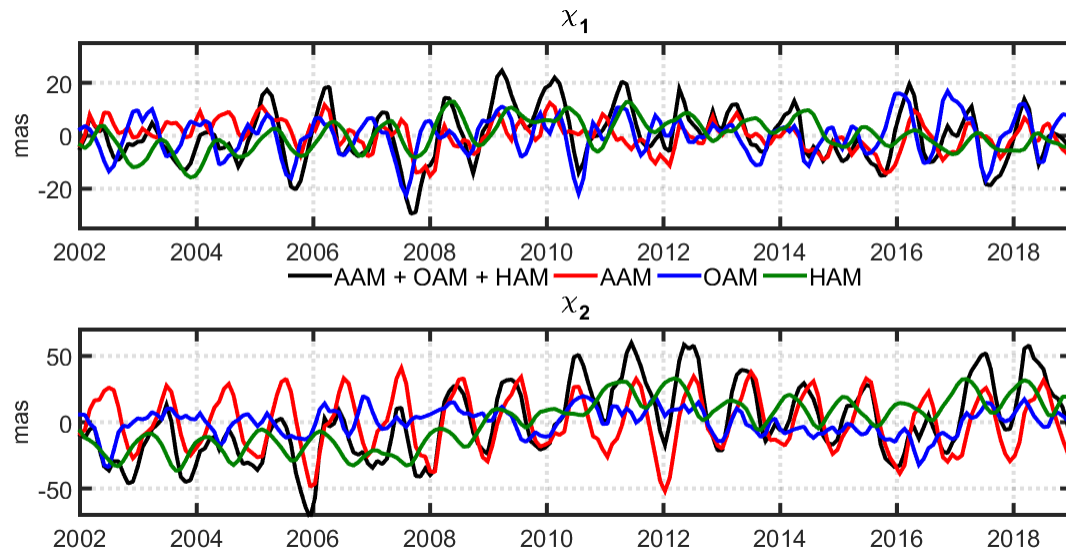


**Fig. 3.** Time series of  $\chi_1$  and  $\chi_2$  components of AAM, OAM and HAM and their sum (AAM+OAM+HAM) computed from geophysical models: ECMWF (for AAM), MPIOM (for OAM), LSDM (for HAM). Each time series was filtered using Gaussian filter with FWHM equal to 60 days

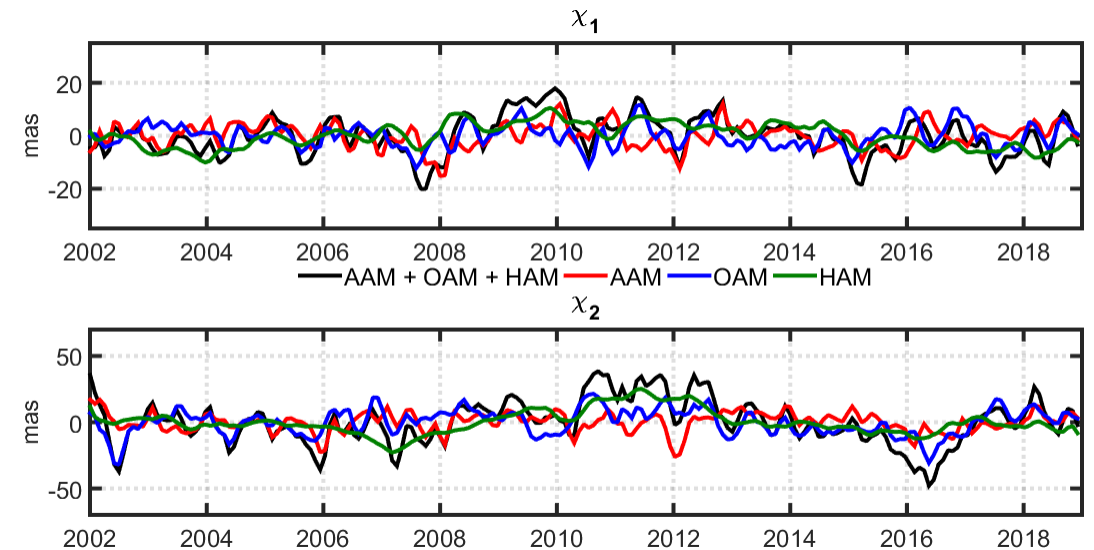


**Fig. 4.** Time series of  $\chi_1$  and  $\chi_2$  components of AAM, OAM and HAM and their sum (AAM+OAM+HAM) computed from geophysical models: ECMWF (for AAM), MPIOM (for OAM), LSDM (for HAM) after removing seasonal variations

# Introduction

## Hydrological excitation of polar motion

- It was previously shown that at seasonal and sub-seasonal scales, the sum of AAM and OAM is responsible for 80 % of PM excitation. The remaining signal in polar motion variations can be explained by HAM, which results from changes in land hydrosphere components, including surface water, soil moisture, snow water, and groundwater, the sum of which is referred to as terrestrial water storage (TWS).
- The impact of atmosphere and ocean on PM has been well established but the role of land hydrosphere is the main source of uncertainties in PM excitation budget.
- The mass variations of land hydrosphere have a smaller impact on precession/nutation and LOD. Moreover, precession and nutation are well described by theoretical models.
- In recent works, hydrological excitation of PM has been estimated from a number of meteorological measurements, global hydrological models, and numerical climate models. Such models are based on observations and simulations of surface water, snow water, ice and soil moisture distribution.
- However, HAM obtained from different data sources exhibited visible discrepancies, both with respect to each other and with respect to the hydrological signal in observed PM excitation, derived from precise geodetic measurements (see Figs. 5 and 6).

# Introduction

## Hydrological excitation of polar motion

- The main reason of discrepancies between diverse models estimations of HAM are differences in meteorological model forcing data, processing algorithms, temporal and spatial resolution or number of parameters estimated.
- Disagreement with observed PM data is caused by the lack of some water storage components or unrealistic simulations of other variables. Additionally, other geophysical effects, such as earthquake-induced co- and post-seismic deformations or Earth's core-mantle coupling are usually not considered in a rigorous way.

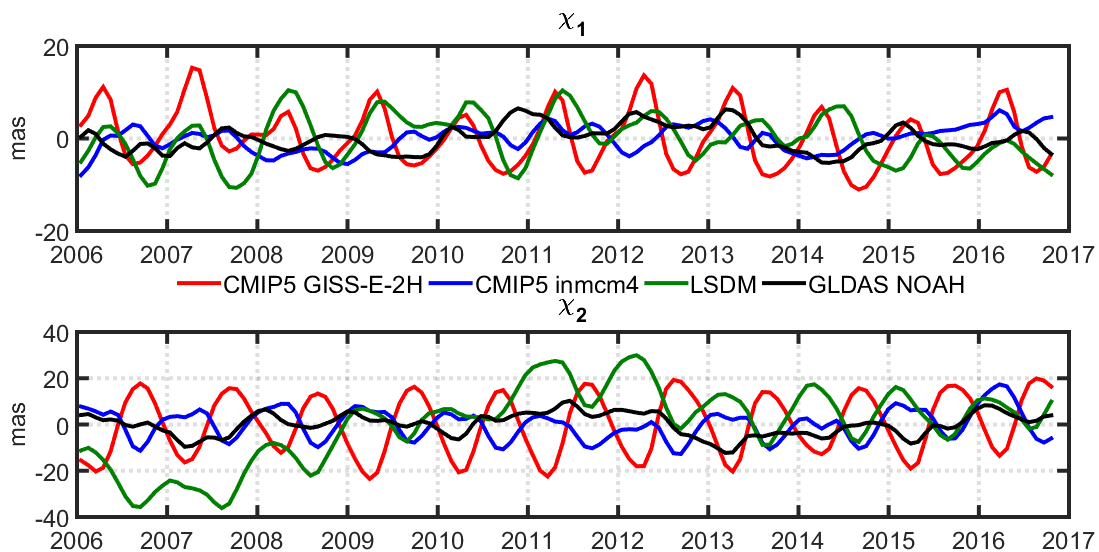


**Fig. 5.** Time series of  $\chi_1$  and  $\chi_2$  components of HAM computed from different hydrological and climate models. Each time series was filtered using Gaussian filter with FWHM equal to 60 days

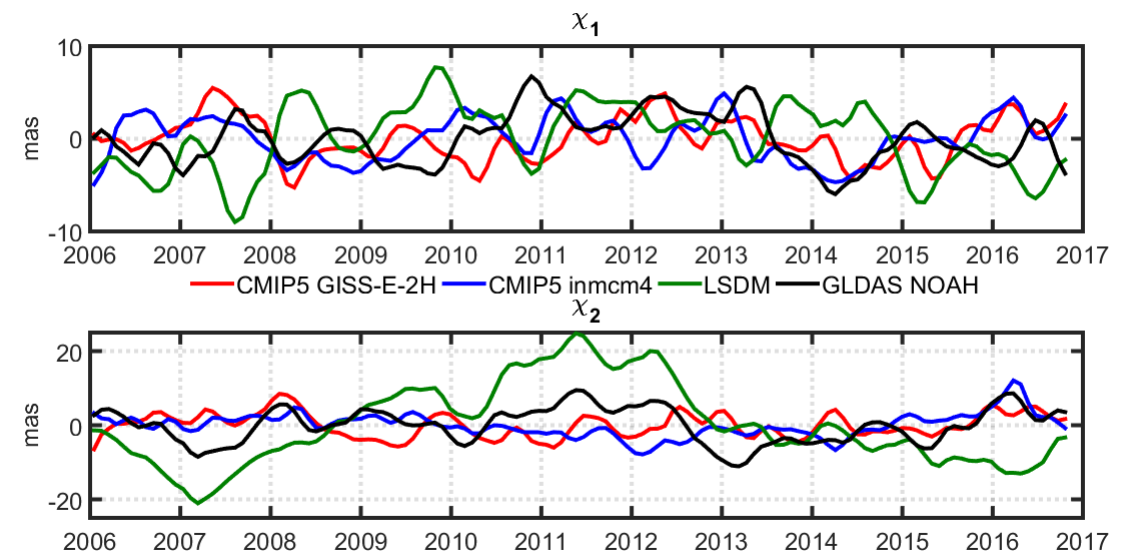


**Fig. 6.** Time series of  $\chi_1$  and  $\chi_2$  components of HAM computed from different hydrological and climate models after removing seasonal variations

# Introduction

## GRACE as a source of data for PM excitation estimation

- Alternative information on PM excitation due to global mass redistribution can be obtained from observations of temporal variations in the gravity field, provided by the **Gravity Recovery and Climate Experiment (GRACE)** mission.
- The GRACE twin-satellites, thanks to mutual measurement of changes in distance between them, provide valuable information on changes in Earth's gravity caused by the variable mass redistribution of surface fluid layers (atmosphere, ocean, land hydrosphere).
- After removing tidal effects as well as non-tidal atmospheric and oceanic contributions from the GRACE-based gravity estimates, the remaining signal is mostly an indication of the land hydrosphere.
- Monthly GRACE datasets are available for the period from April 2002 to June 2017 (163 months, with occasional gaps).



Image credit: <https://grace.jpl.nasa.gov/resources/12/grace-logo/>

# Introduction

## GRACE as a source of data for PM excitation estimation

- The variations of **degree-2, order-1 spherical harmonic coefficients ( $\Delta C_{21}$ ,  $\Delta S_{21}$ )** of GRACE-based geopotential models are commonly used in determination of mass-related PM excitation. It is possible, because changes of  $\Delta C_{21}$ ,  $\Delta S_{21}$  are proportional to the variations of  $\chi_1$  and  $\chi_2$  equatorial components of the PM excitation. PM excitation series obtained in that way indicate the impact of the land hydrosphere, but also glacial isostatic adjustment (GIA), barystatic sea-level contributions, and earthquake signatures.
- Another method is to exploit **Terrestrial Water Storage (TWS) anomalies given in regular grids**. Such GRACE data products are obtained from spherical harmonic coefficients of all degrees and orders, after appropriate reprocessing (filtering, correcting due to GIA, replacing  $C_{20}$  with an estimate from SLR, correcting degree-1 coefficients). They provide information about changes in water content on lands. Consequently, the resulting PM excitation series describe the effects from continental water, without GIA or barystatic sea-level changes.
- The third method is based on **mass concentration blocks (or “mascons”, MAS)**. In contrast to spherical harmonics-based TWS anomalies, mascon-based TWS variations are given in blocks with known geophysical location. Such solutions do not need to be destripped or smoothed.
- The PM excitation caused by land hydrosphere and obtained from the GRACE observations are sometimes denoted as **gravimetric–hydrological excitation, gravimetric excitation**, or simply **GRACE-based HAM**.

# Introduction

## GRACE as a source of data for PM excitation estimation

- The great success and scientific sound of the GRACE mission, which ended in 2017, contributed to the launch of its successor, **GRACE Follow-On (GRACE-FO or GFO)** in May 2018. Until now, monthly time series of both GRACE- and GFO-based geopotential models have been made available to the users by official GRACE data centers at Center for Space Research (CSR), Jet Propulsion Laboratory (JPL) and GeoForschungsZentrum (GFZ).

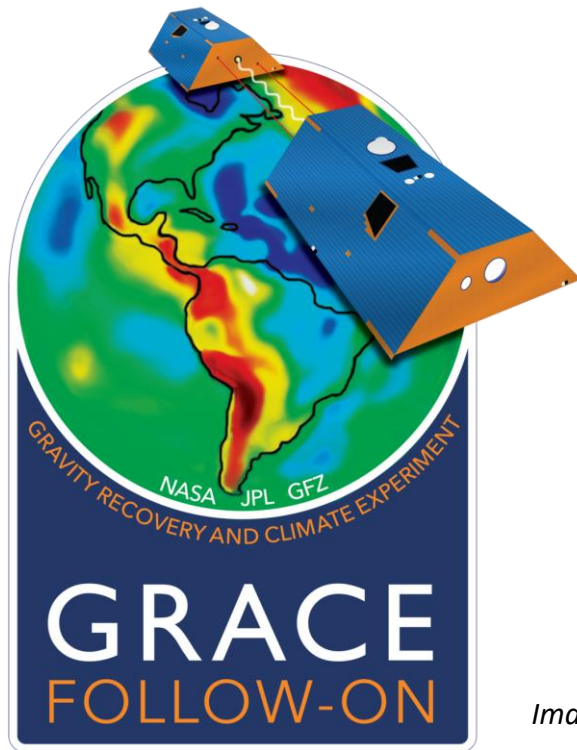


*Image credit: GFZ Potsdam*

- To date, monthly GFO datasets have been made available for the period from June 2018 to February 2020 (21 months).

# Introduction

## Validation of HAM

- A common method to validate HAM estimates (either model-based or GRACE-based) is to compare them with hydrological signal in observed PM excitation, derived from precise geodetic measurements.
- To do this, observed GAM series should be reduced for the effects of atmosphere and ocean to study only the residual signals, denoted as **geodetic residuals** (GAM–AAM–OAM or GAO):

$$\text{GAO} = \text{GAM} - \text{AAM} - \text{OAM},$$

where GAM, AAM and OAM are geodetic angular momentum, atmospheric angular momentum and oceanic angular momentum, respectively. GAM is computed from precise coordinates of the pole, while AAM and OAM are based on models of atmosphere and ocean.

- The resulting series (GAO) are expected to represent the impact of land hydrosphere and barystatic sea-level changes on PM excitation. Nevertheless, it should be kept in mind that GAO will also contain signals from changes in the mass of ice sheets, the effects of large earthquakes, and the signatures of geomagnetic jerks.

# Motivation and objectives

# Motivation and objectives

- **The aim of this study is to present first estimates of hydrological excitation of PM (Hydrological Angular Momentum, HAM) obtained from new GRACE Follow-On mission.**
- To compute HAM, we use: (1)  $C_{21}$ ,  $S_{21}$  coefficients of geopotential, (2) gridded TWS anomalies, and (3) mascon solutions.
- We compare and evaluate the three methods of HAM estimation and examine the compatibility between CSR, JPL and GFZ solutions.
- We also validate different HAM estimations using precise geodetic measurements of the pole coordinates (GAO).
- By comparing with HAM obtained from previous GRACE mission, we try to assess the updates and improvements in mass-related PM excitation.

# Motivation and objectives

The analyses are divided into three parts:

1. Internal agreement between GRACE– and GFO–based hydrological polar motion excitation estimates
2. External validation of GRACE– and GFO–based hydrological polar motion excitation estimates
3. Comparison between  $C_{21}$ ,  $S_{21}$ –based, TWS–based and mascon-based HAM

# Data and methods

# Data and methods

## GRACE/GRACE-FO data types

### 1. Spherical harmonics coefficients (or GSM coefficients or Stokes coefficients) of the Earth's geopotential (Level-2 GRACE data)

- $\chi_1, \chi_2$  components of PM excitation are proportional to the changes of  $C_{21}, S_{21}$  coefficients of geopotential (Gross, 2015):

$$\chi_1 = -\sqrt{\frac{5}{3}} \cdot \frac{1.608 \cdot R_e^2 \cdot M}{C - A'} \Delta C_{21}$$

$$\chi_2 = -\sqrt{\frac{5}{3}} \cdot \frac{1.608 \cdot R_e^2 \cdot M}{C - A'} \Delta S_{21}$$

where  $R_e$  and  $M$  are the Earth's mean Earth's radius and mass, respectively;  $A, B,$  and  $C$  are the principal moments of inertia for Earth;  $A' = (A + B)/2$  is an average of the equatorial principal moments of inertia; and  $\Delta C_{21}$  and  $\Delta S_{21}$  are the normalized spherical harmonics coefficients of the gravity field (Table 1 in Gross, 2015);

- The signals from glacial isostatic adjustment (GIA), earthquakes, barystatic sea-level changes due to inflow of water from lands into oceans are not removed;
- Some residual signals from ocean (due to ocean model errors) are retained.

# Data and methods

## GRACE/GRACE-FO data types

### 2. Terrestrial Water Storage (TWS) gridded data (Level-3 GRACE data)

- TWS anomalies are given in regular grid;
- Obtained from spherical harmonics of all degrees and orders after filtering and applying corrections: GIA correction,  $C_{20}$  replaced with values from Satellite Laser Ranging (SLR), degree-1 coefficients correction;
- $\chi_1, \chi_2$  can be computed by summing up the effects from TWS ( $\Delta q$ ) over lands:

$$\chi_1 = -\frac{1.098R_e^2}{C - A} \iint \Delta q(\varphi, \lambda, t) \sin \varphi \cos \varphi \cos \lambda dS$$

$$\chi_2 = -\frac{1.098R_e^2}{C - A} \iint \Delta q(\varphi, \lambda, t) \sin \varphi \cos \varphi \sin \lambda dS$$

where  $\Delta q(\varphi, \lambda, t)$  are changes in water storage,  $R_e$  is Earth's mean radius,  $dS$  is the surface area and  $C$  and  $A$  are Earth's principal moments of inertia. The factor 1.098 accounts for the yielding of the solid Earth to surface load, rotational deformation and core-mantle decoupling (*Eubanks, 1993*);

- The use of land mask allow to separate land signals. In the result,  $\chi_1, \chi_2$  express only the impact of land hydrosphere on polar motion excitation.

# Data and methods

## GRACE/GRACE-FO data types

### 3. Mascon (MAS) solutions (Level-3 GRACE data)

- Not based on spherical harmonics but mass concentration blocks (or “mascons”). TWS anomalies are given in each mascon with known geophysical location (*Wiese et al., 2016, Watkins et al., 2015*);
- The filtration is not needed. The GIA,  $C_{20}$ , degree-1 coefficients corrections are applied;
- $\chi_1, \chi_2$  can be computed by summing up the effects from TWS ( $\Delta q$ ) over lands:

$$\chi_1 = -\frac{1.098R_e^2}{C - A} \iint \Delta q(\varphi, \lambda, t) \sin \varphi \cos \varphi \cos \lambda dS$$

$$\chi_2 = -\frac{1.098R_e^2}{C - A} \iint \Delta q(\varphi, \lambda, t) \sin \varphi \cos \varphi \sin \lambda dS$$

where  $\Delta q(\varphi, \lambda, t)$  are changes in water storage,  $R_e$  is Earth’s mean radius,  $dS$  is the surface area and  $C$  and  $A$  are Earth’s principal moments of inertia. The factor 1.098 accounts for the yielding of the solid Earth to surface load, rotational deformation and core-mantle decoupling (*Eubanks, 1993*);

- The use of land mask allow to separate land signals. In the result,  $\chi_1, \chi_2$  express only the impact of land hydrosphere on polar motion excitation.

# Data and methods

## GRACE/GRACE-FO data used

For Level-2 GRACE/GRACE-FO data, we used **3 monthly spherical harmonics (GSM) solutions** provided by the following data centers:

- Jet Propulsion Laboratory (JPL), Pasadena, USA — **JPL RL06** solution,
- Center for Space Research (CSR), Austin, USA — **CSR RL06** solution,
- GeoForschungsZentrum (GFZ), Potsdam, Germany — **GFZ RL06** solution.

For Level-3 GRACE data, we used **3 monthly TWS solutions** (obtained from spherical harmonics) provided by the following data centers:

- Jet Propulsion Laboratory (JPL), Pasadena, USA — **JPL RL06** solution,
- Center for Space Research (CSR), Austin, USA — **CSR RL06** solution,
- GeoForschungsZentrum (GFZ), Potsdam, Germany — **GFZ RL06** solution,

and **one mascon (MAS) solution**:

- From Jet Propulsion Laboratory (JPL), Pasadena, USA — **JPL RL06M v02** solution.

# Data and methods

## Data used for GAO computation

- **$\chi_1$  and  $\chi_2$  equatorial components of GAM:** based on daily combined 14 C04 series of EOP derived from GNSS, SLR, and VLBI. EOP 14 C04 series are fully consistent with the International Terrestrial Reference Frame 2014 (ITRF 2014). The EOP data are provided by the International Earth Rotation and Reference System Service (IERS) (<https://www.iers.org/IERS/EN/DataProducts/EarthOrientationData/eop.html>) and updated on a regular basis. The series are available at temporal resolution of 24 h. In this study, for computation of GAM, we used an algorithm given at <http://hpiers.obspm.fr/eop-pc/index.php?index=excitactive&lang=en>;
- **$\chi_1$  and  $\chi_2$  equatorial components of AAM:** provided by the GFZ, and based on ECMWF (European Center for Medium-Range Weather Forecasts) model. The series are available at temporal resolution of 3 h and can be accessed from <http://rz-vm115.gfz-potsdam.de:8080/repository>. Note that the current AAM version provided by GFZ is consistent with GRACE AOD1B RL06 Atmosphere and Ocean De-Aliasing Level-1B Release-6 (AOD1B RL06);
- **$\chi_1$  and  $\chi_2$  equatorial components of OAM:** provided by the GFZ, and based on MPIOM (Max Planck Institute Ocean Model). The series are available at temporal resolution of 3 h and can be accessed from <http://rz-vm115.gfz-potsdam.de:8080/repository>. Note that the current OAM version provided by GFZ is consistent with GRACE AOD1B RL06.

# Results

# Internal agreement

## Time series

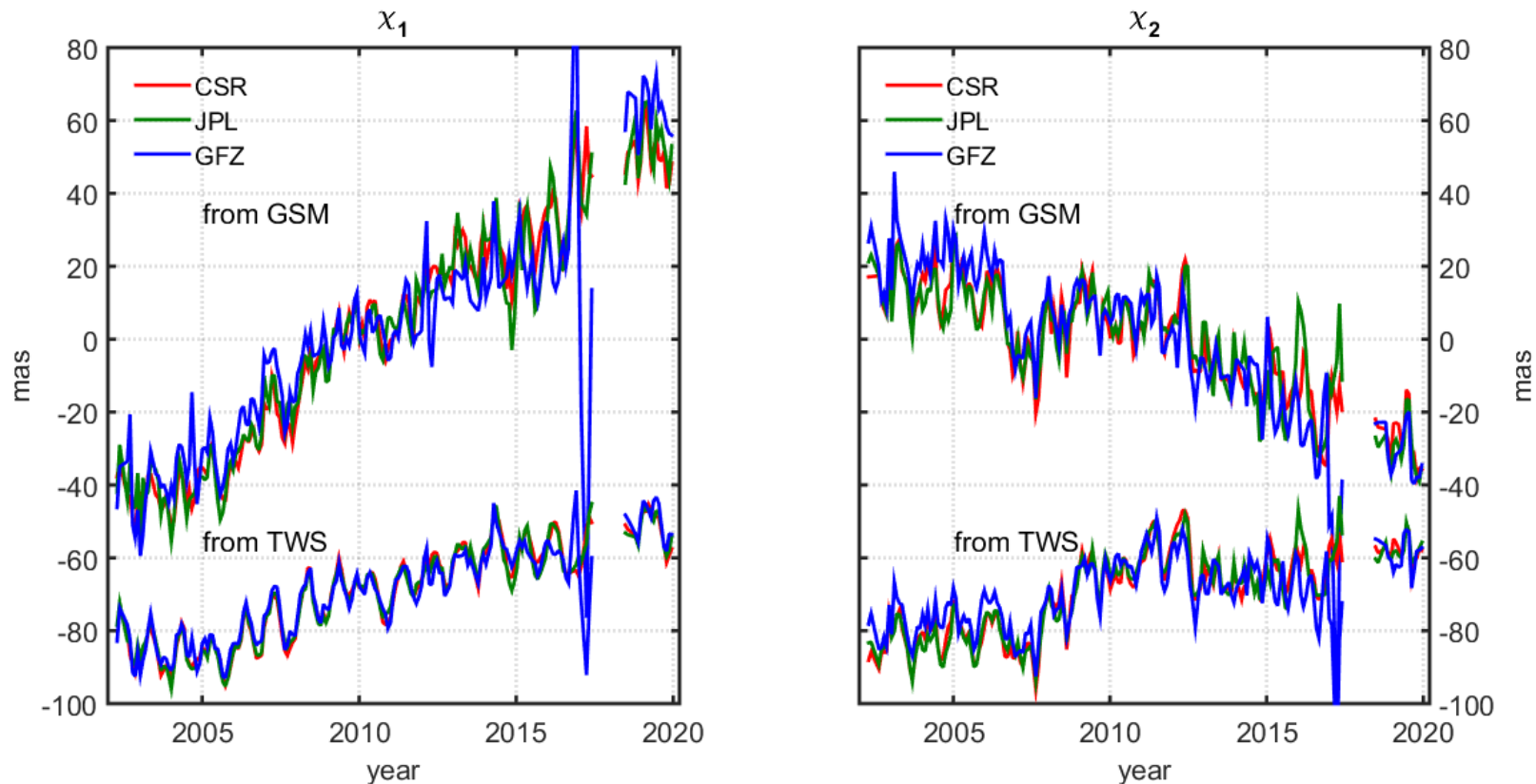


**Fig. 7.** Time series of  $\chi_1$  and  $\chi_2$  components of HAM computed from GRACE and GRACE-FO monthly solutions: Level-2 data (GSM) and Level-3 data (TWS)

*The trend differences between HAM from GSM and HAM from TWS are mainly due to applying GIA model in TWS data (which is not used in GSM). Post-glacial rebound primarily affects PM trends.*

*GRACE-based HAM series are more consistent with each other when Level-3 TWS data is used.*

**Tab. 1.** (a) Standard deviation of HAM series (in mas), (b) Trends in HAM series (in mas/year)

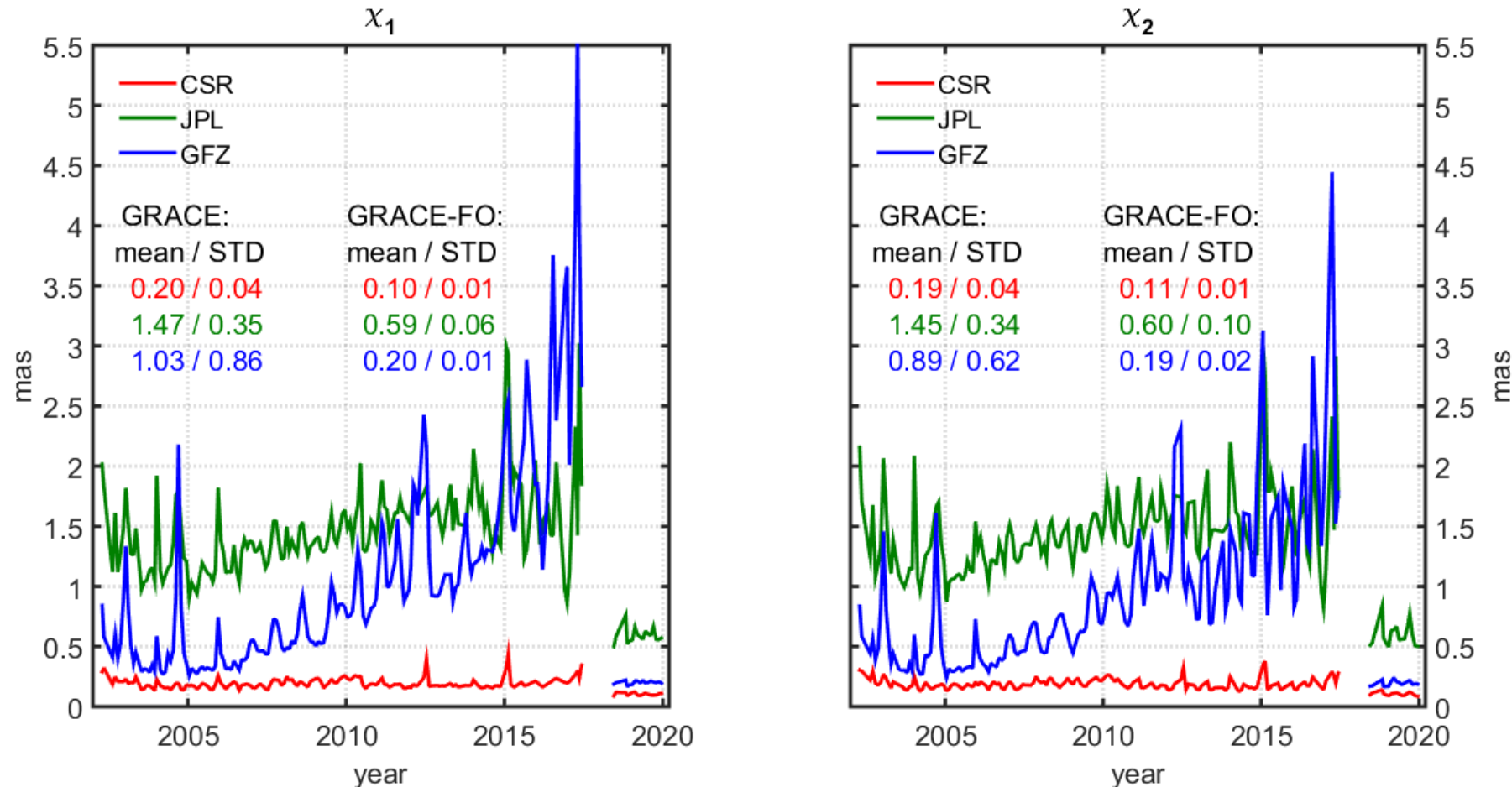
a)		GRACE		GRACE-FO	
		$\chi_1$	$\chi_2$	$\chi_1$	$\chi_2$
CSR	GSM	7.33	8.98	5.62	5.89
JPL	GSM	8.76	9.39	7.07	5.86
GFZ	GSM	15.82	11.86	6.20	5.79
CSR	TWS	5.83	7.51	4.18	3.01
JPL	TWS	5.92	7.45	4.17	2.74
GFZ	TWS	6.60	8.86	4.38	4.25

b)		GRACE		GRACE-FO	
		$\chi_1$	$\chi_2$	$\chi_1$	$\chi_2$
CSR	GSM	6.38	-2.33	-3.16	-6.33
JPL	GSM	6.05	-2.07	0.15	-3.11
GFZ	GSM	4.67	-3.79	-2.75	-8.25
CSR	TWS	2.40	1.87	-3.48	-0.54
JPL	TWS	2.36	1.91	-1.07	1.90
GFZ	TWS	2.05	0.86	-1.99	-1.91

# Internal agreement

## Formal errors



*The best GRACE performance takes place in 2006–2013.*

*During the entire GRACE operational period, some peaks of visibly higher errors occurs, typically related to occasional periods of short repeat orbits.*

*Compared to other GRACE data, the CSR series has the lowest and the most stable errors.*

*After 2005, the errors of GFZ-based HAM series start to increase linearly.*

*The errors for GRACE-FO are definitely smaller and less noisy than errors for GRACE.*

**Fig. 8.** Errors of  $\chi_1$  and  $\chi_2$  components of HAM obtained from GRACE Level-2 data. The errors are computed from formal errors of  $C_{21}$ ,  $S_{21}$  coefficients. Mean errors and STD of errors are added for each time series. All values are given in mas

# Internal agreement

## Comparison with mean GRACE/GRACE-FO

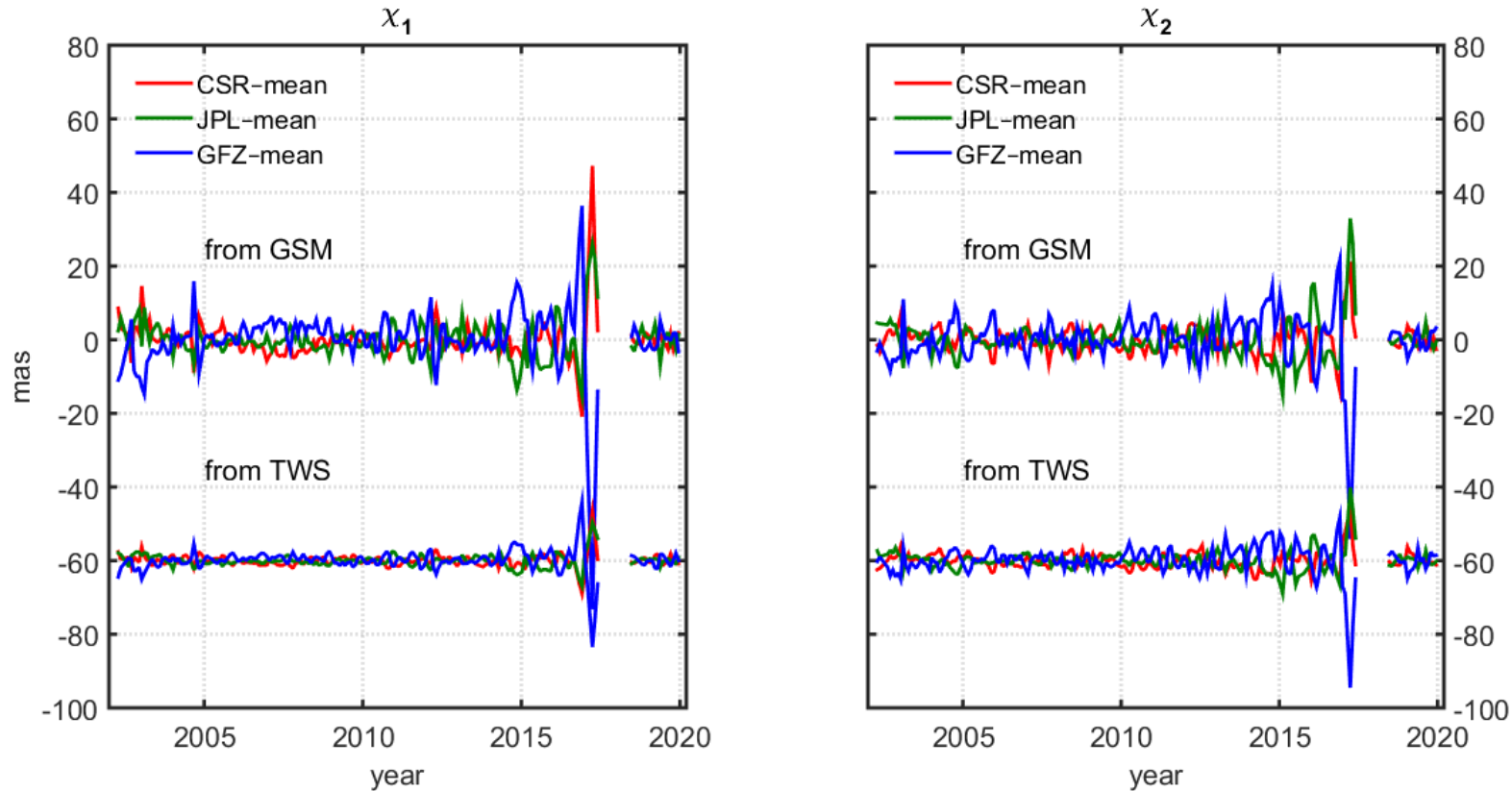


**Fig. 9.** Differences between HAM obtained from a particular GRACE/GRACE-FO solution and HAM computed from mean GRACE/GRACE-FO (mean of CSR, JPL and GFZ solutions)

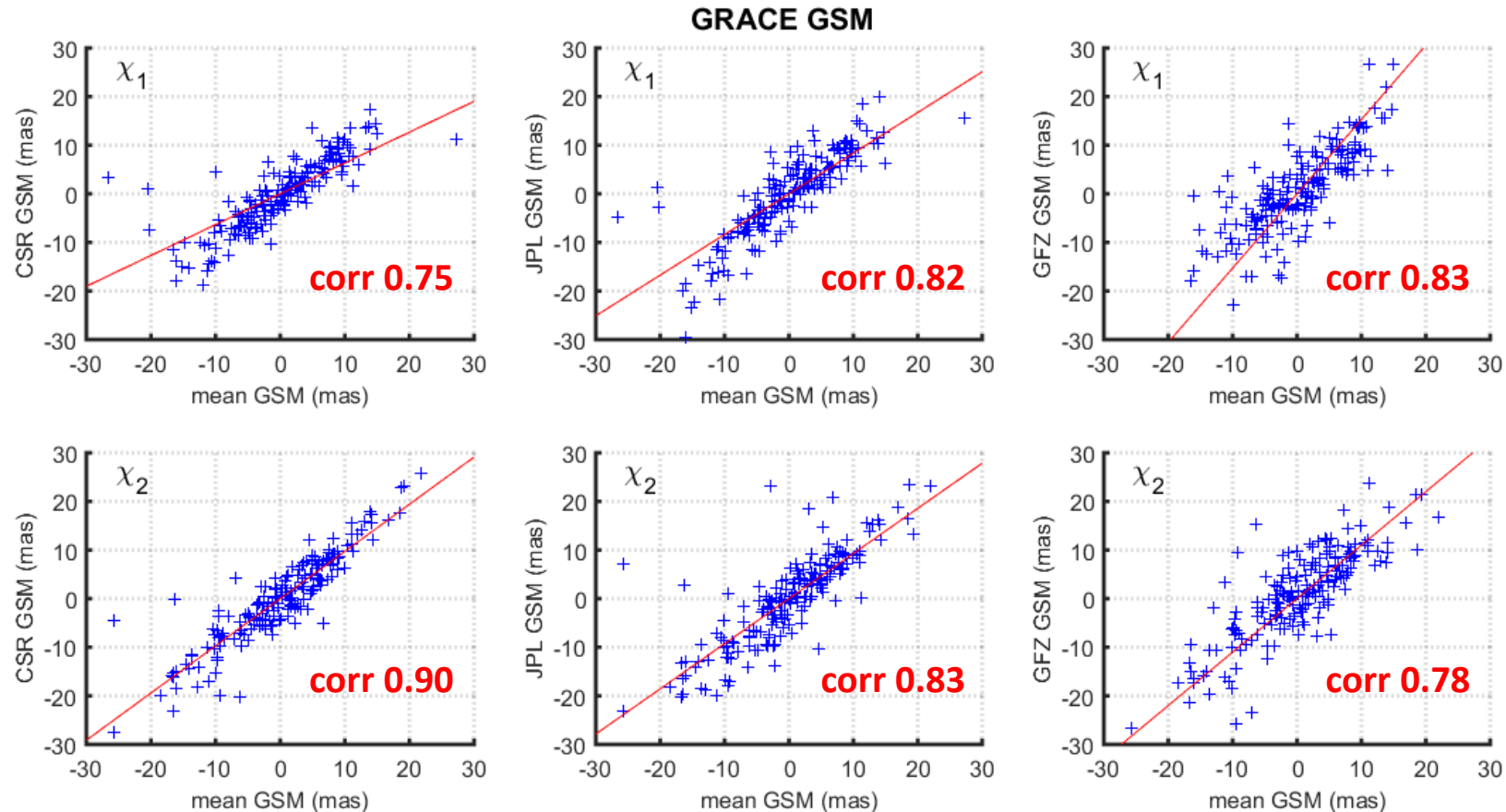
**Tab. 2.** RMS of differences (root-mean-square errors, RMSE) between HAM from a particular GRACE/GRACE-FO solution and HAM from mean GRACE/GRACE-FO (mean of CSR, JPL and GFZ solutions)

		GRACE		GRACE-FO	
		$x_1$	$x_2$	$x_1$	$x_2$
CSR	GSM	5.80	3.85	1.50	1.79
JPL	GSM	5.17	5.31	2.48	1.52
GFZ	GSM	9.85	7.52	2.37	2.48
CSR	TWS	1.86	2.38	0.89	1.35
JPL	TWS	1.84	2.92	0.67	1.14
GFZ	TWS	3.28	4.48	1.21	2.04

*The GRACE and GRACE-FO series from GFZ deviate the most from the average.  
GRACE/GRACE-FO-based HAM series are more consistent with the mean when the Level-3 TWS datasets are used.*

# Internal agreement

## Comparison with mean GRACE/GRACE-FO



*The closer the points are to the red line, the higher the relationship between the time series is.*

**Fig. 10.** Scatter plots showing the relationship between HAM from particular GRACE/GRACE-FO solutions and HAM from mean GRACE/GRACE-FO solution. The values in red indicate correlation coefficients between series. The red line was fitted to the data points using the least squares method

# Internal agreement

## Comparison with mean GRACE/GRACE-FO

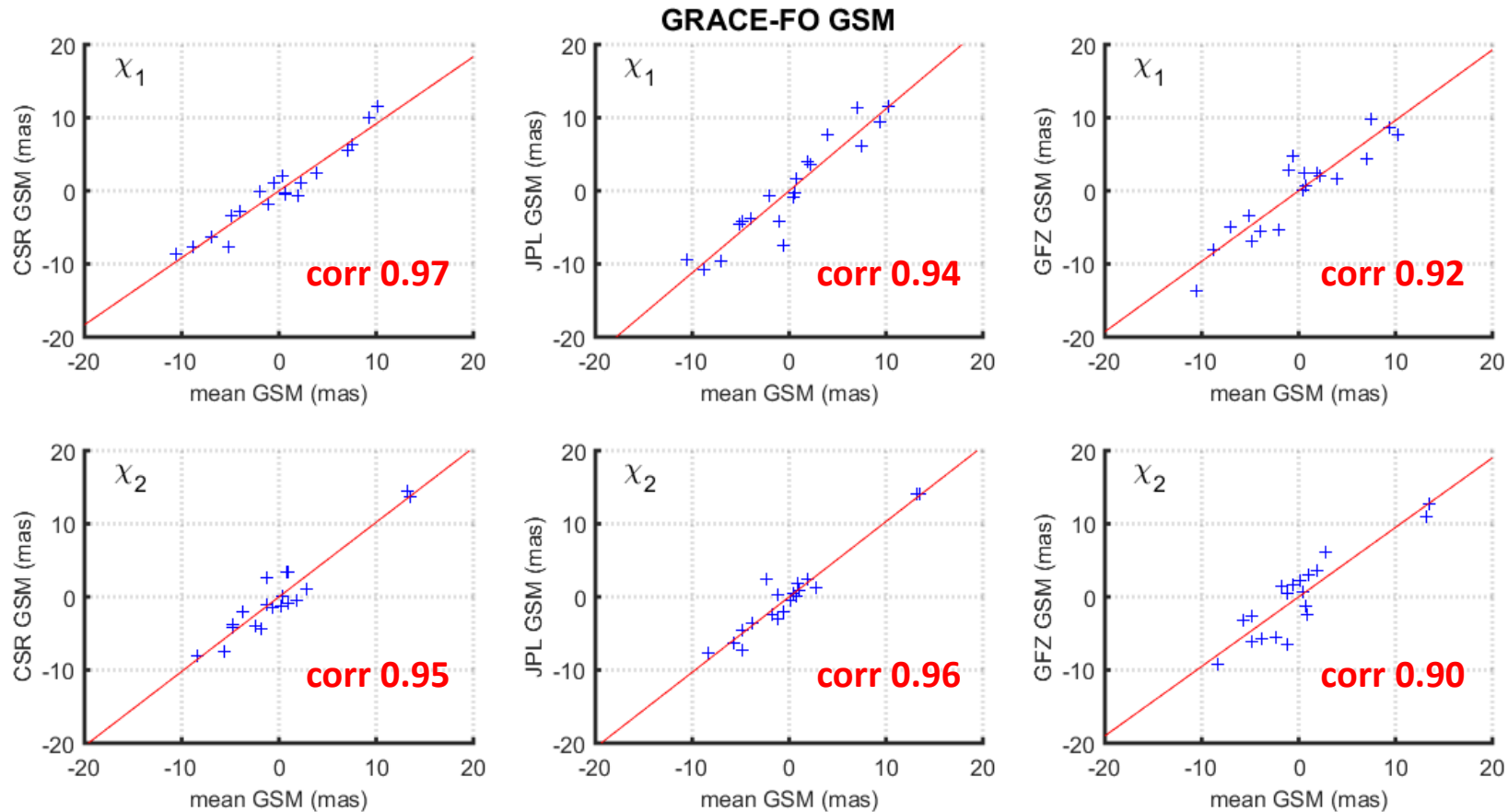


**Fig. 11.** Scatter plots showing the relationship between HAM from particular GRACE/GRACE-FO solutions and HAM from mean GRACE/GRACE-FO solution. The values in red indicate correlation coefficients between series. The red line was fitted to the data points using the least squares method

# Internal agreement

## Comparison with mean GRACE/GRACE-FO

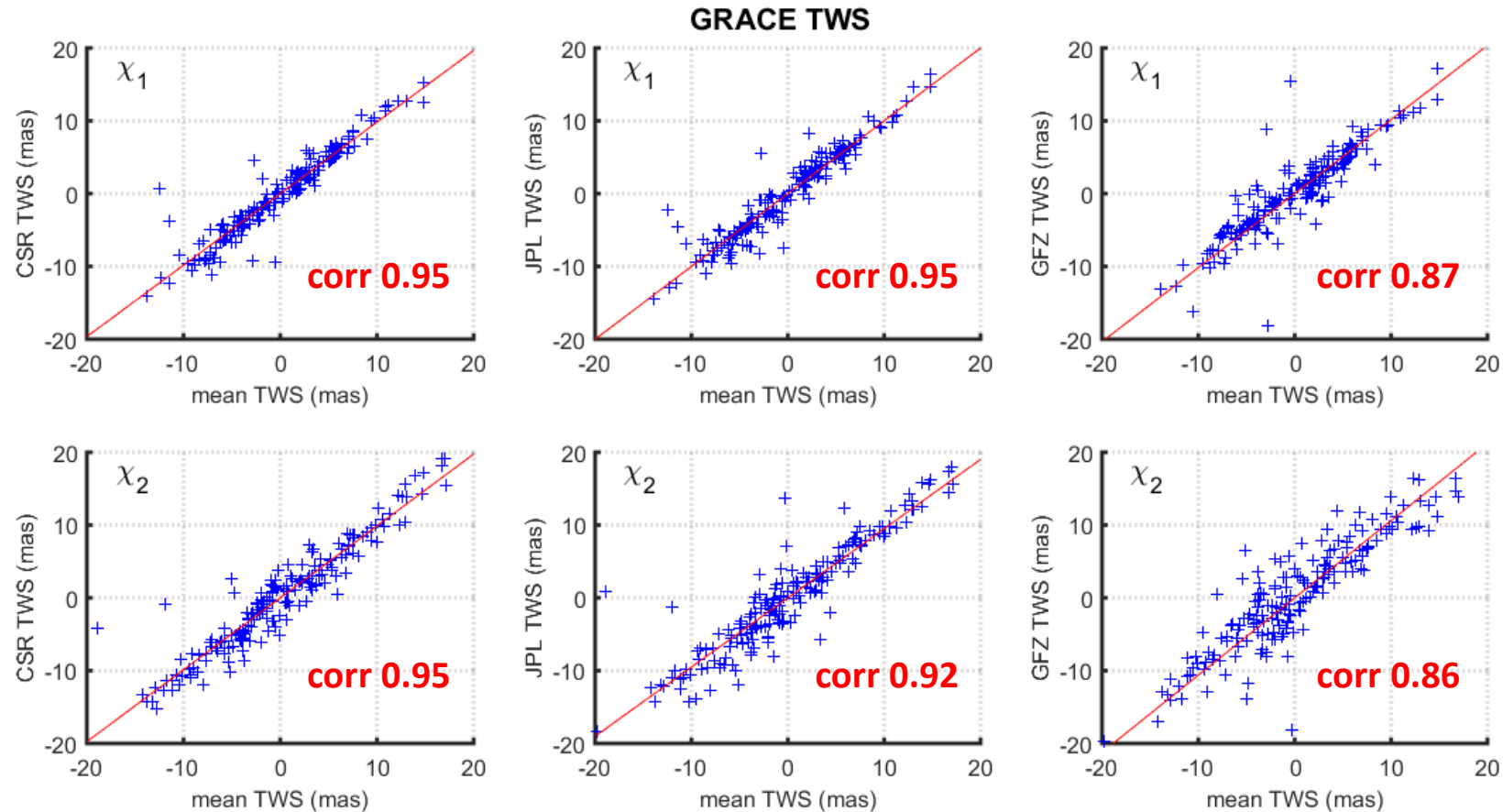
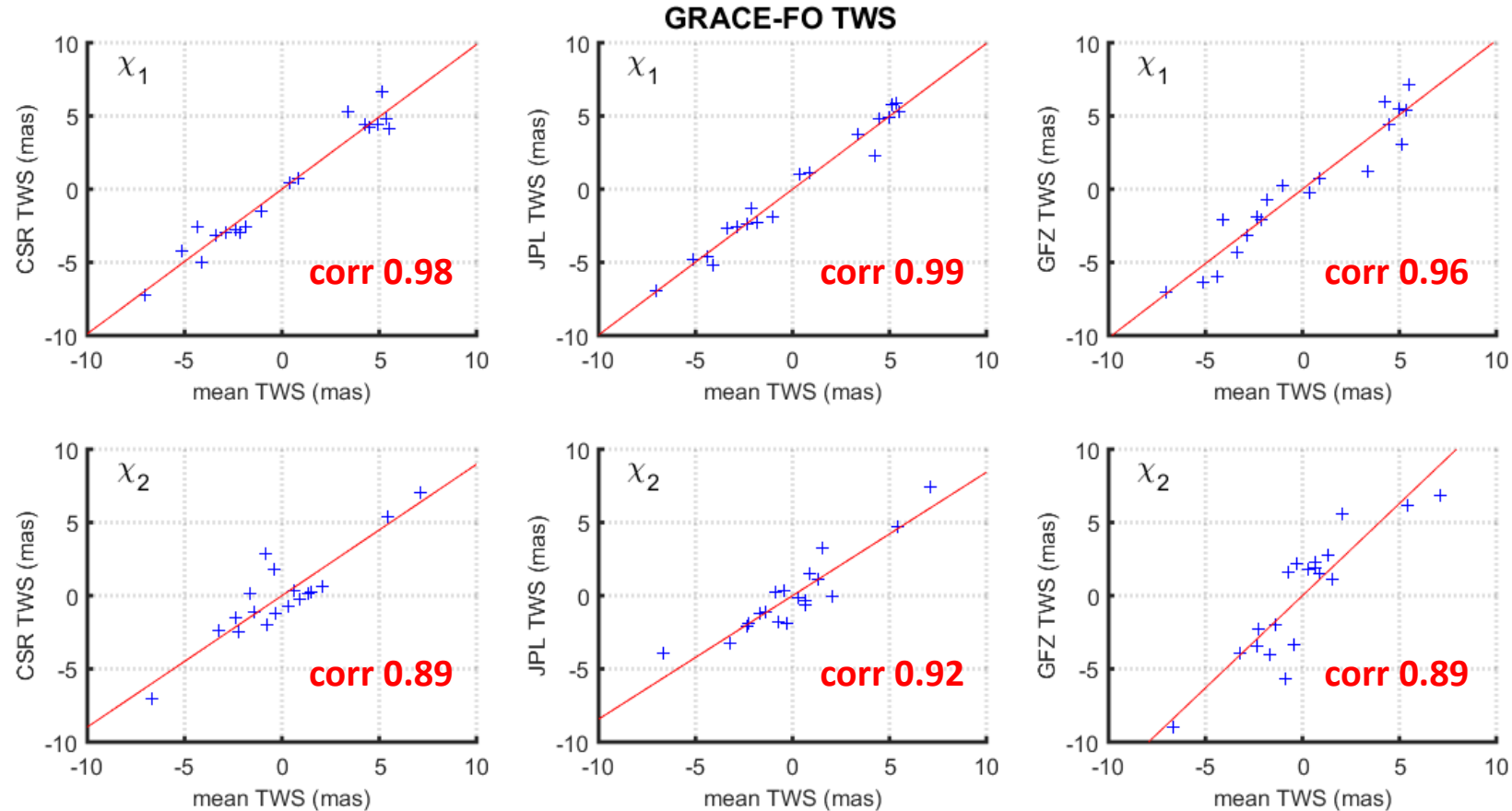


**Fig. 12.** Scatter plots showing the relationship between HAM from particular GRACE/GRACE-FO solutions and HAM from mean GRACE/GRACE-FO solution. The values in red indicate correlation coefficients between series. The red line was fitted to the data points using the least squares method

# Internal agreement

## Comparison with mean GRACE/GRACE-FO



The correlations between HAM from particular GRACE/GRACE-FO solutions and HAM from mean GRACE/GRACE-FO solution are higher when Level-3 TWS data are used.

**Fig. 13.** Scatter plots showing the relationship between HAM from particular GRACE/GRACE-FO solutions and HAM from mean GRACE/GRACE-FO solution. The values in red indicate correlation coefficients between series. The red line was fitted to the data points using the least squares method

# Internal agreement

## Comparison between particular GRACE/GRACE-FO solutions

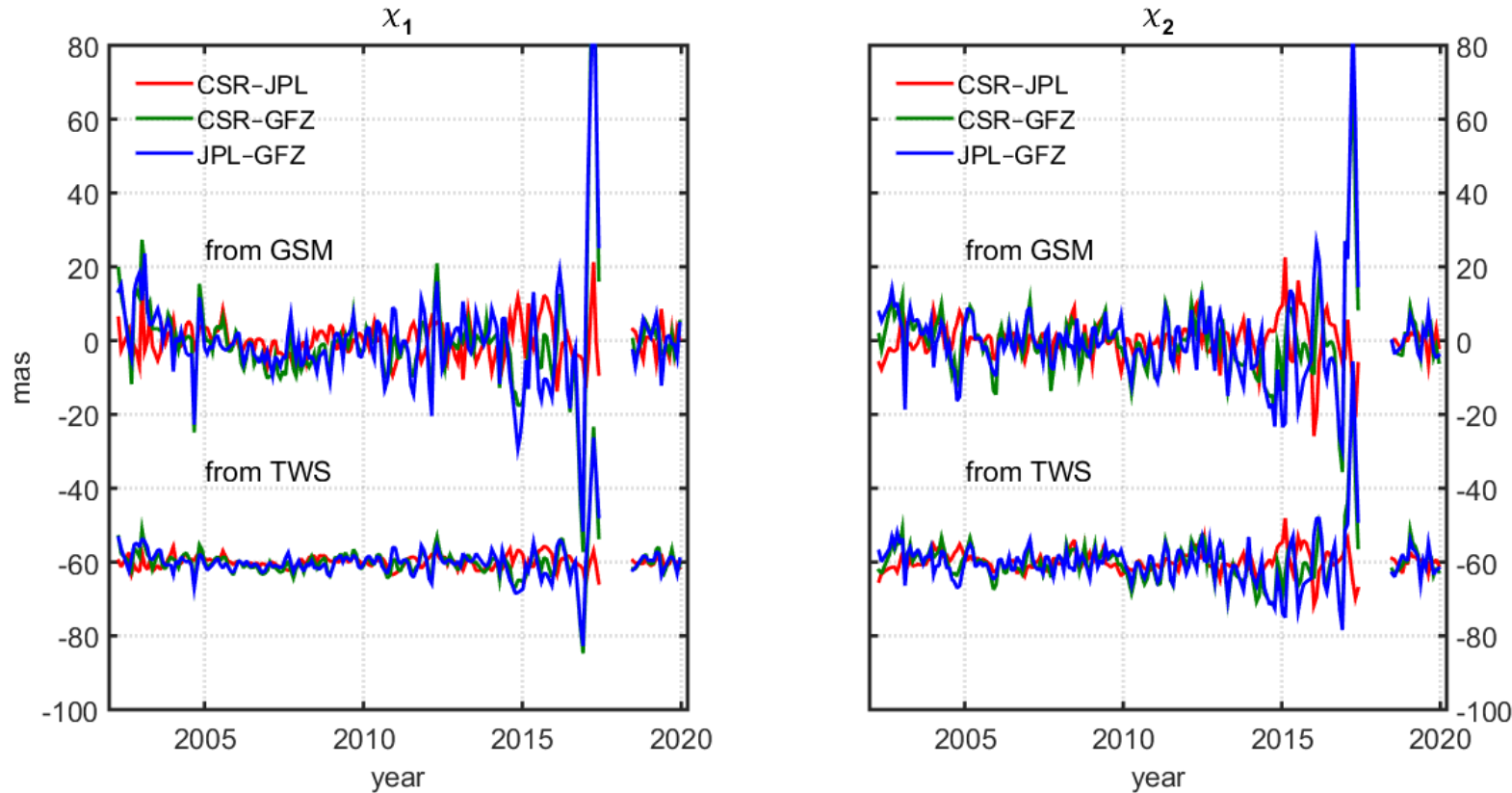


Fig. 14. Differences between HAM obtained from particular GRACE/GRACE-FO solutions

Tab. 3. RMS of differences (root-mean-square errors, RMSE) between HAM from particular GRACE/GRACE-FO solutions

		GRACE		GRACE-FO	
		$\chi_1$	$\chi_2$	$\chi_1$	$\chi_2$
CSR/JPL	GSM	4.86	5.42	3.34	2.21
CSR/GFZ	GSM	15.32	10.70	3.10	4.04
JPL/GFZ	GSM	14.63	12.43	4.61	3.70
CSR/JPL	TWS	1.71	2.89	1.00	1.43
CSR/GFZ	TWS	5.00	6.55	2.01	3.26
JPL/GFZ	TWS	4.99	7.18	1.74	3.01

*The lowest errors are obtained when GRACE/GRACE-FO data from CSR and JPL are compared.*

*GRACE/GRACE-FO-based HAM series are more consistent with each other when Level-3 TWS data are used.*

*HAM from particular GRACE/GRACE-FO solutions are more compatible for  $\chi_2$  than for  $\chi_1$ .*

# Internal agreement

## Comparison between particular GRACE/GRACE-FO solutions

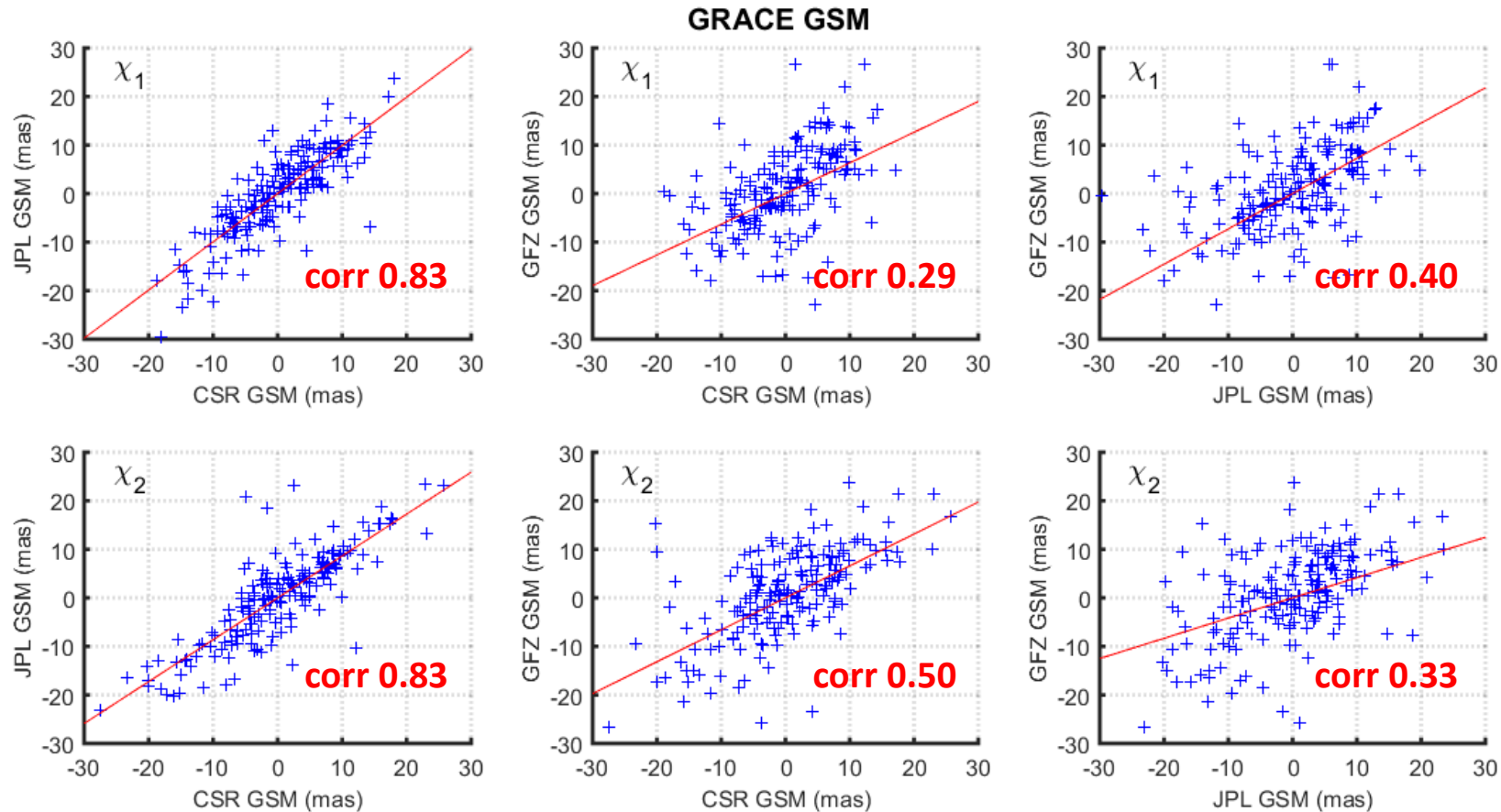


**Fig. 15.** Scatter plots showing the relationship between HAM from particular GRACE/GRACE-FO solutions. The values in red indicate correlation coefficients between series. The red line was fitted to the data points using the least squares method

# Internal agreement

## Comparison between particular GRACE/GRACE-FO solutions

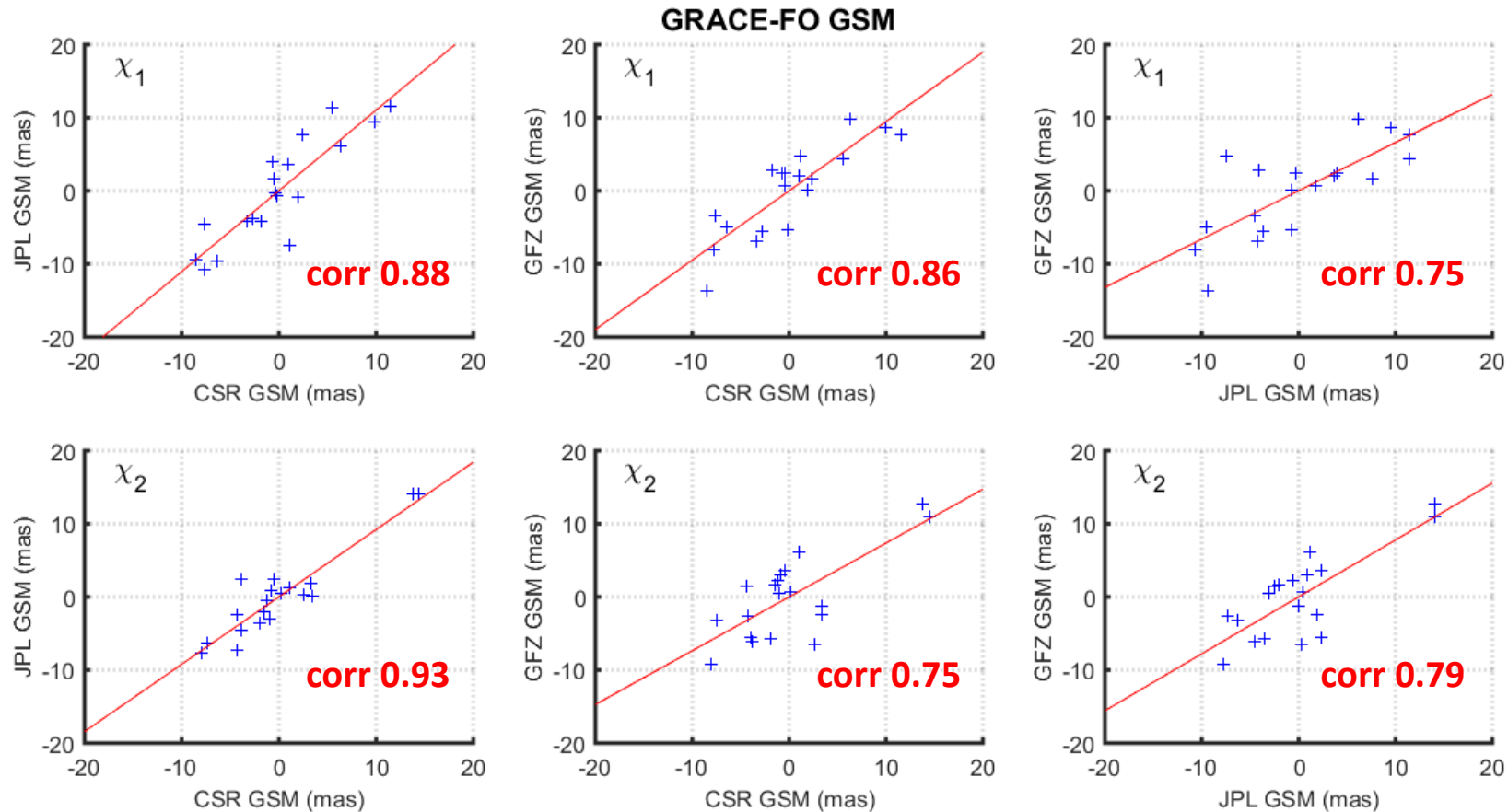


**Fig. 16.** Scatter plots showing the relationship between HAM from particular GRACE/GRACE-FO solutions. The values in red indicate correlation coefficients between series. The red line was fitted to the data points using the least squares method

# Internal agreement

## Comparison between particular GRACE/GRACE-FO solutions

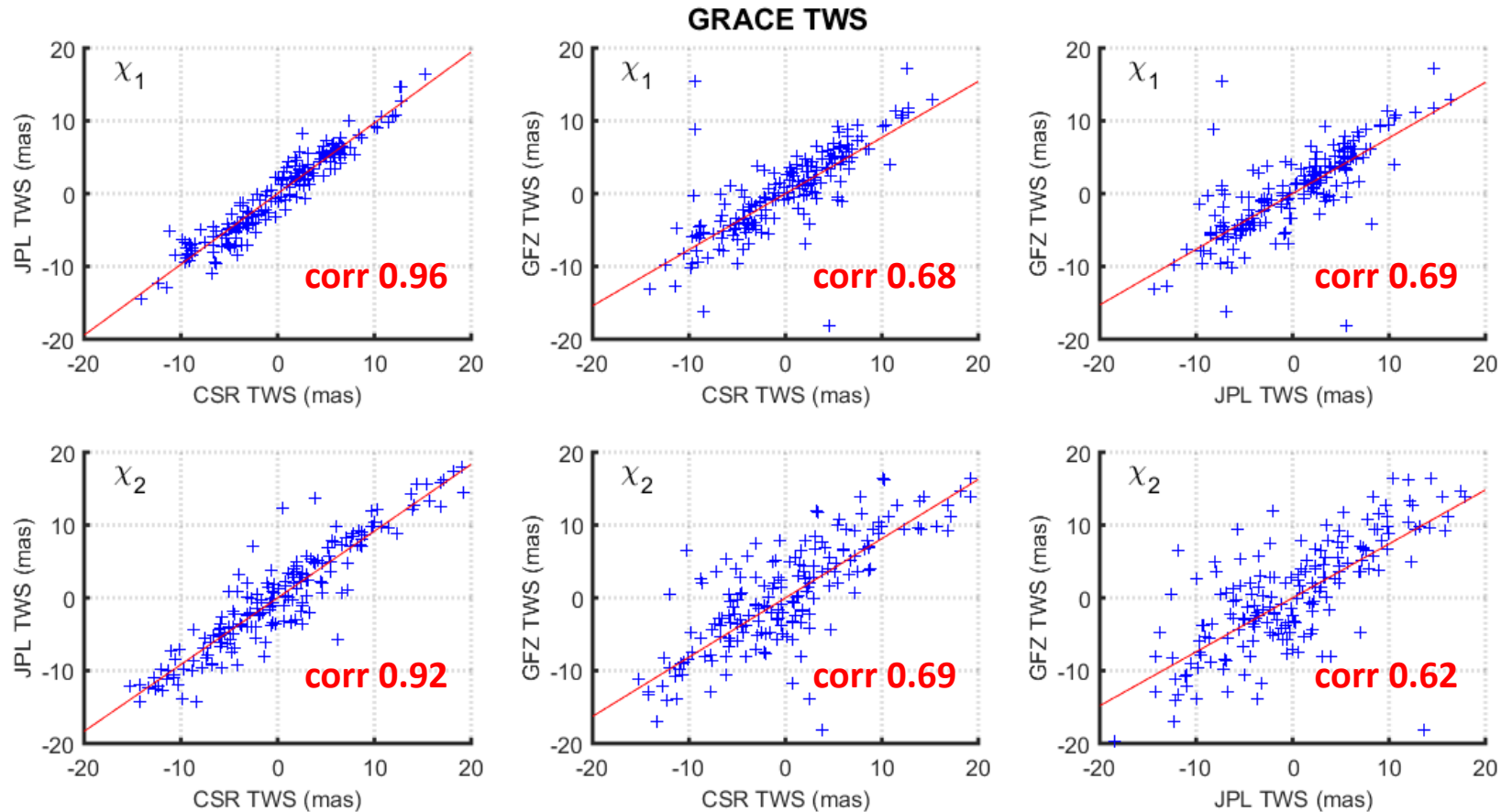
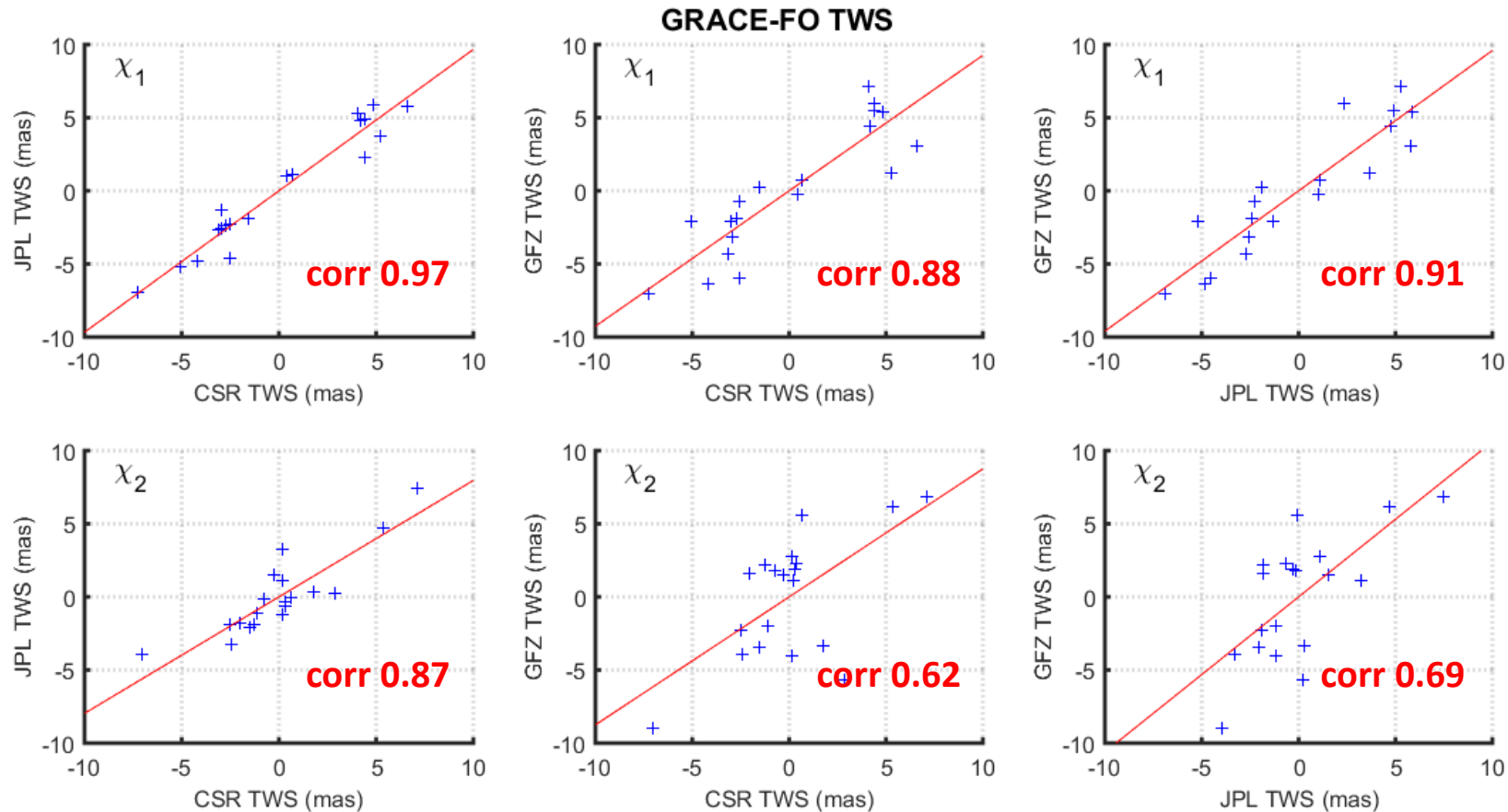


**Fig. 17.** Scatter plots showing the relationship between HAM from particular GRACE/GRACE-FO solutions. The values in red indicate correlation coefficients between series. The red line was fitted to the data points using the least squares method

# Internal agreement

## Comparison between particular GRACE/GRACE-FO solutions



Scatter plots and correlation values prove the highest dependence between CSR and JPL for both GRACE and GRACE-FO, and both Level-2 and Level-3 data.

**Fig. 18.** Scatter plots showing the relationship between HAM from particular GRACE/GRACE-FO solutions. The values in red indicate correlation coefficients between series. The red line was fitted to the data points using the least squares method

# Internal agreement

## Spatial variability: STD

2003: initial period of the GRACE mission

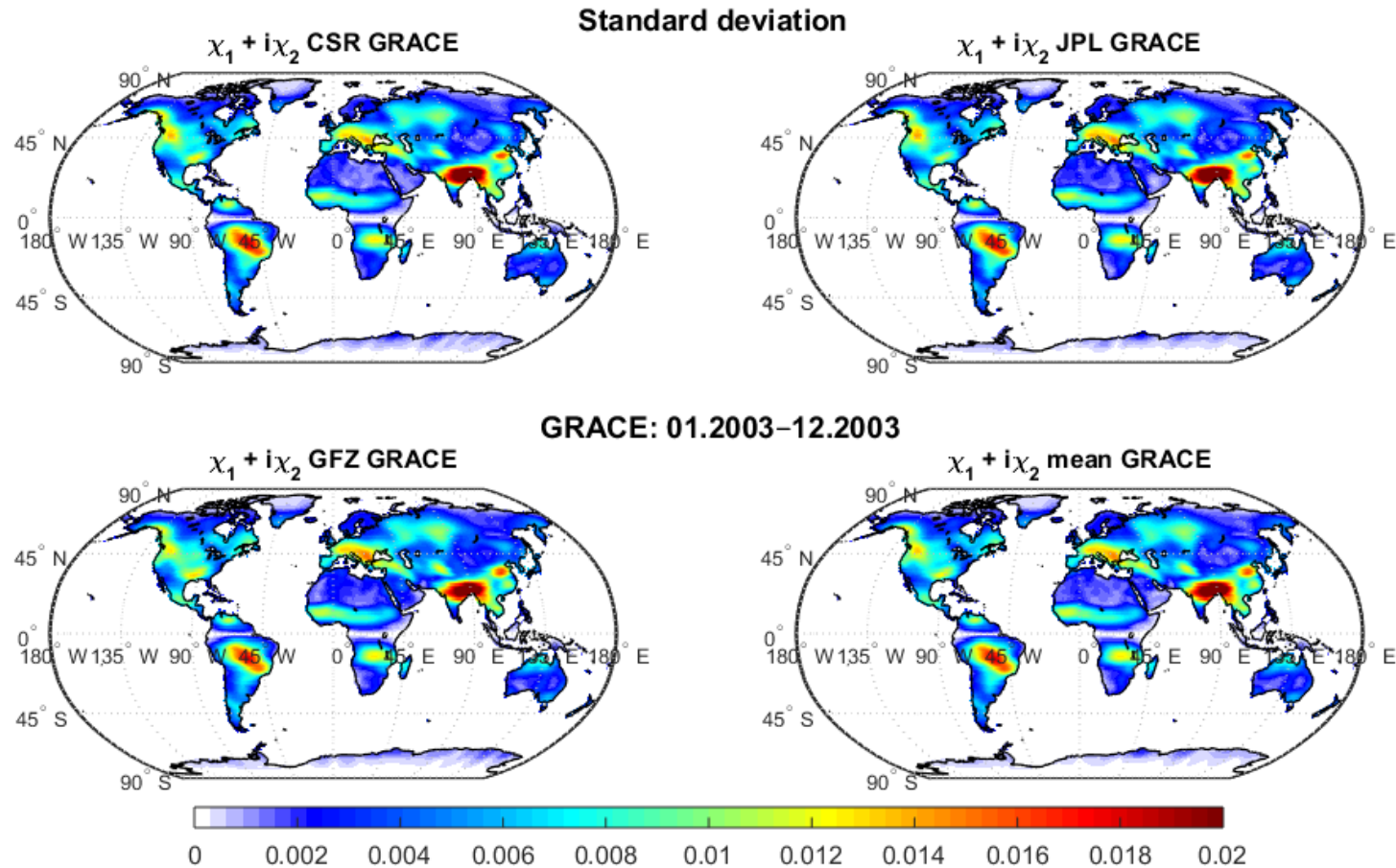


**Fig. 19.** Maps of STD of  $\chi_1 + i\chi_2$  for HAM obtained from GRACE/GRACE-FO Level-3 (TWS) data from CSR, JPL, GFZ and from mean GRACE/GRACE-FO (mean of data from CSR, JPL and GFZ). The values are given in mas

# Internal agreement

## Spatial variability: STD

2006: best GRACE performance

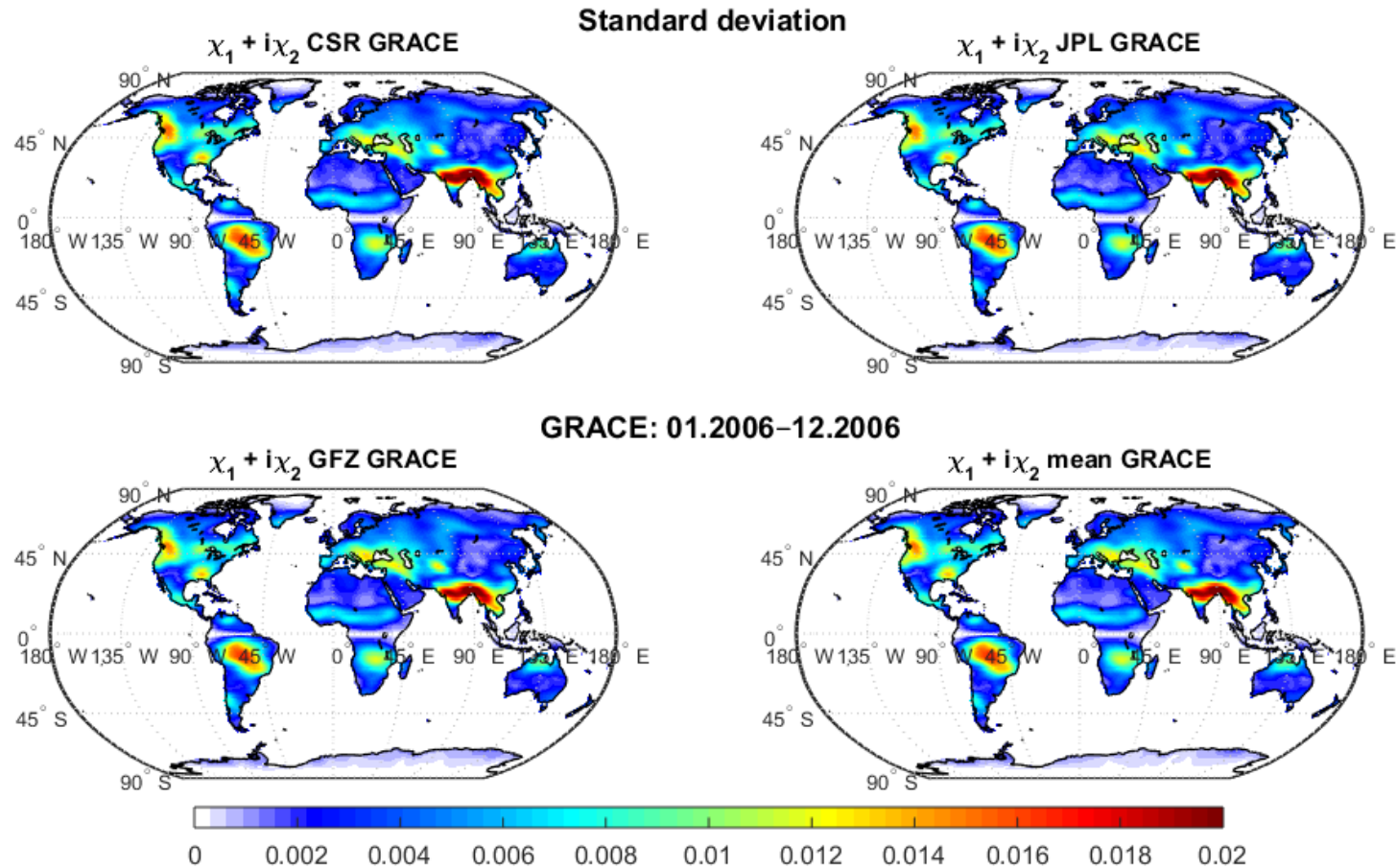
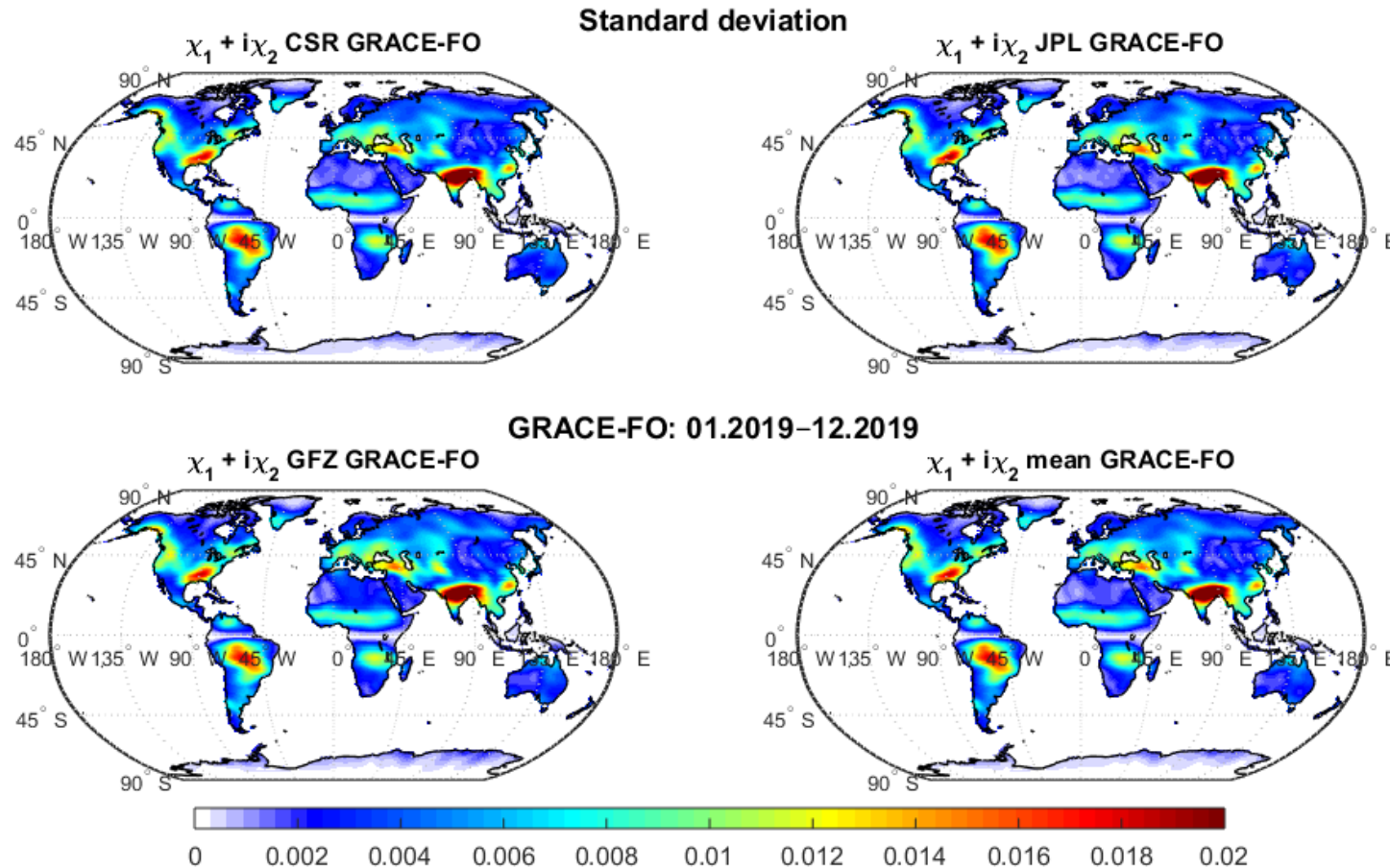


**Fig. 20.** Maps of STD of  $\chi_1 + i\chi_2$  for HAM obtained from GRACE/GRACE-FO Level-3 (TWS) data from CSR, JPL, GFZ and from mean GRACE/GRACE-FO (mean of data from CSR, JPL and GFZ). The values are given in mas

# Internal agreement

## Spatial variability: STD

2019: initial period of the GRACE-FO mission



*The highest variability of HAM is observed in the Amazon basin, the Gulf of Alaska, Himalayas, Southeast Asia, and the Middle East.*

*Spatial variability of HAM is similar for all GRACE and GRACE-FO data.*

*In the initial period of the GRACE (2003) and GRACE-FO (2019), STD of  $\chi_1+i\chi_2$  is quite stronger in Europe and Siberia than in 2006.*

**Fig. 21.** Maps of STD of  $\chi_1 + i\chi_2$  for HAM obtained from GRACE/GRACE-FO Level-3 (TWS) data from CSR, JPL, GFZ and from mean GRACE/GRACE-FO (mean of data from CSR, JPL and GFZ). The values are given in mas

# Internal agreement

## Spatial variability: RMS of differences

2003: initial period of the GRACE mission

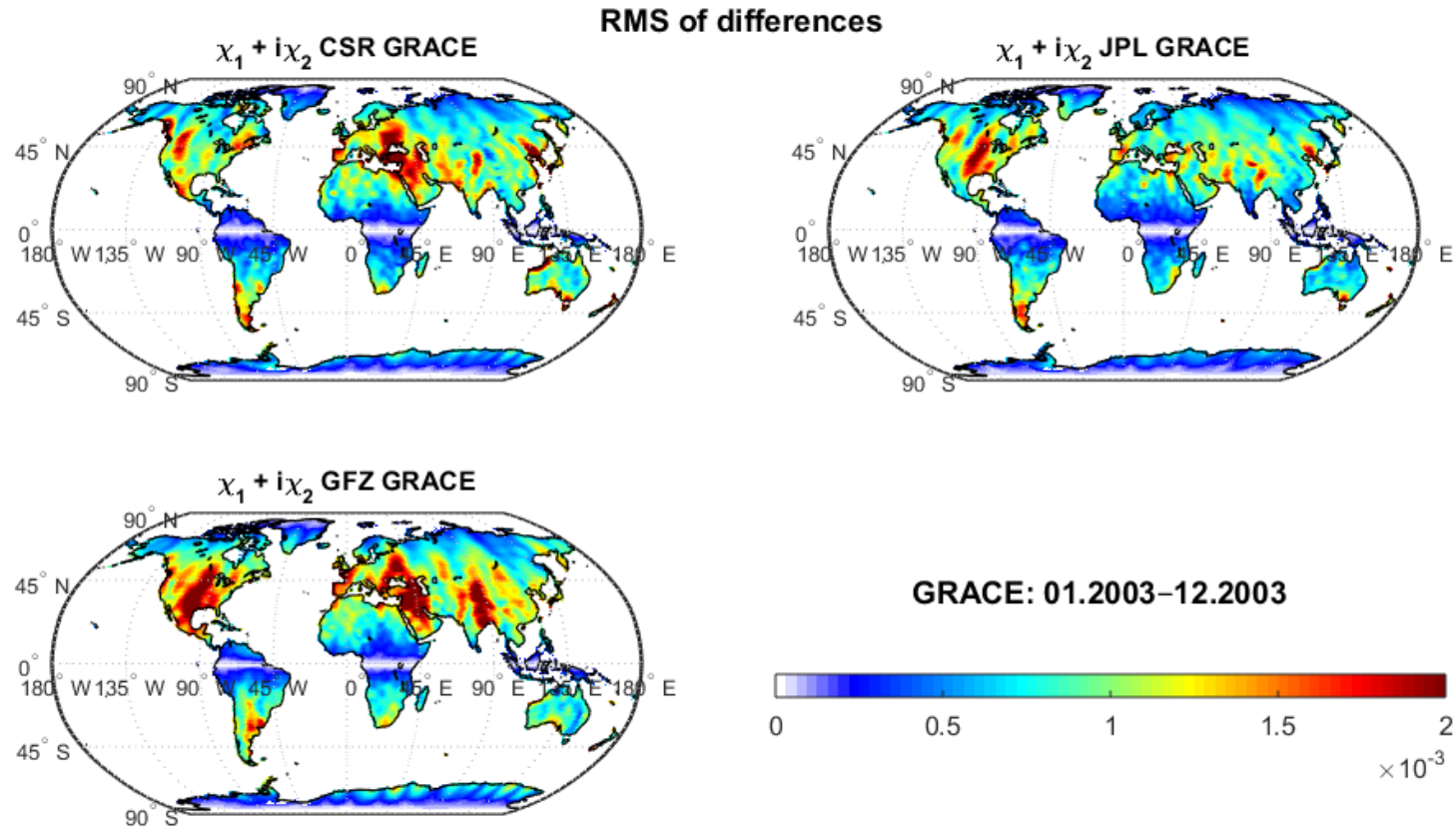


**Fig. 22.** Maps of RMS of differences between HAM from particular GRACE/GRACE-FO solutions and HAM from mean GRACE/GRACE-FO solution. The values are given in mas

# Internal agreement

## Spatial variability: RMS of differences

2006: best GRACE performance

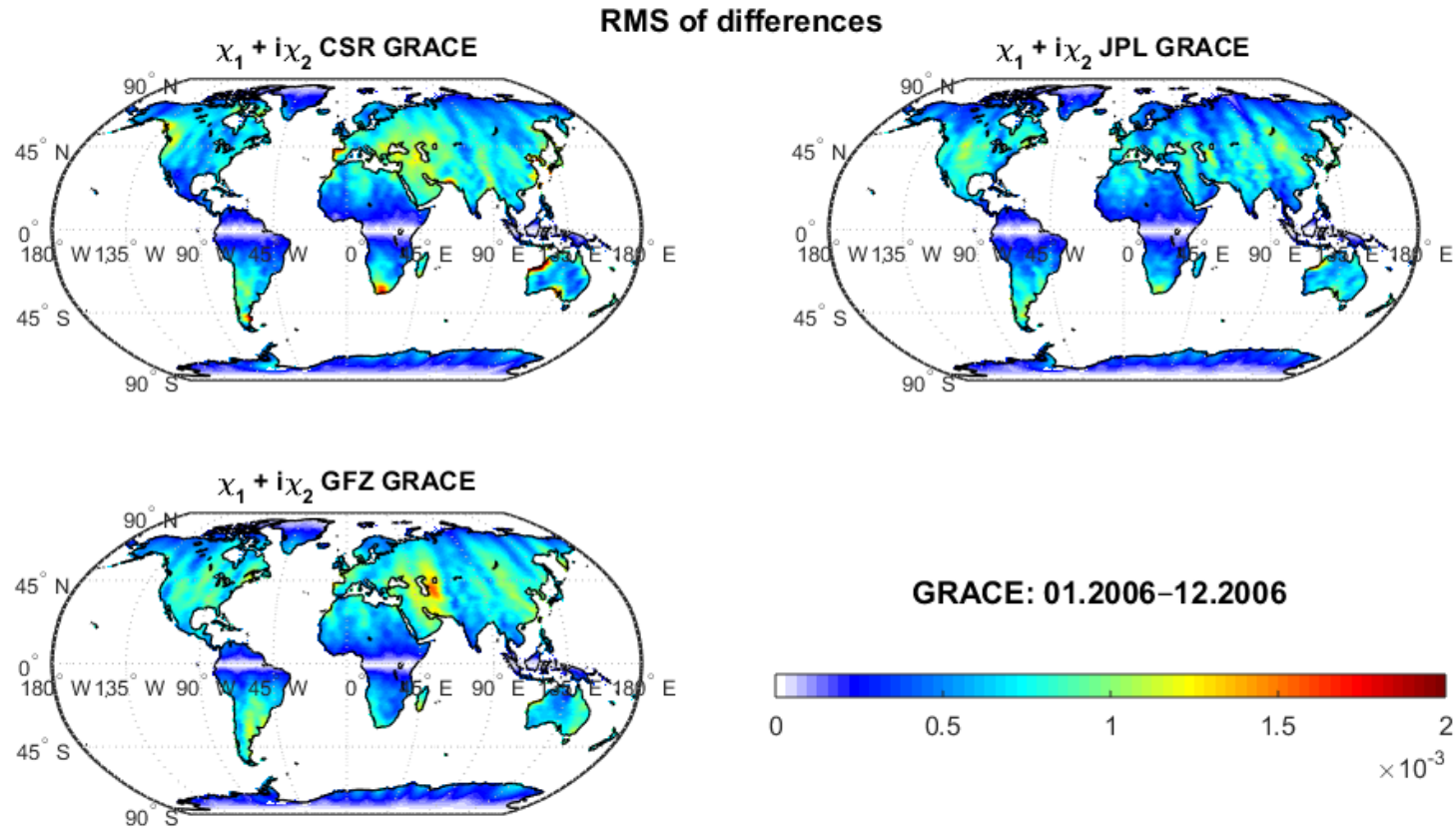
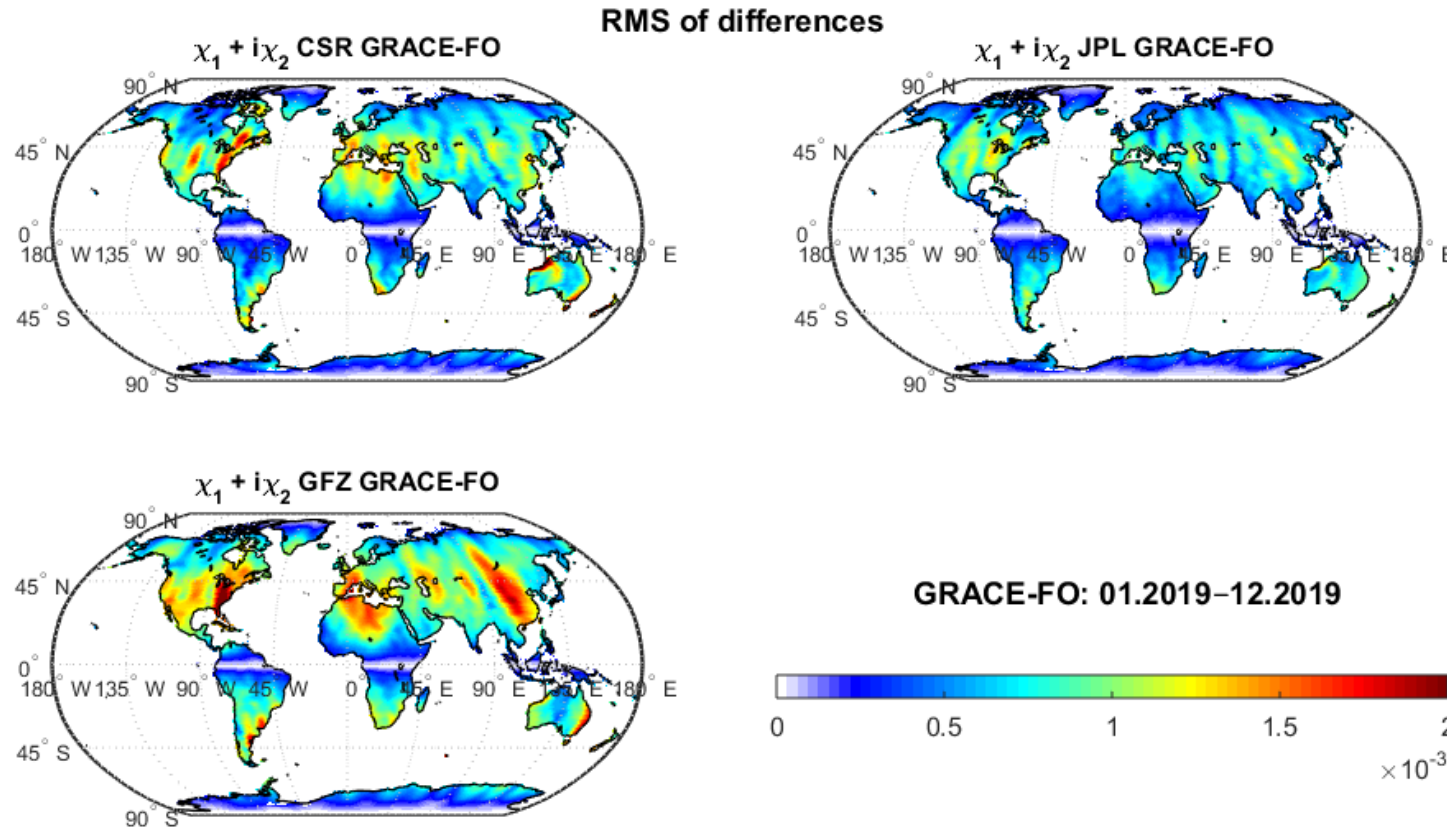


**Fig. 23.** Maps of RMS of differences between HAM from particular GRACE/GRACE-FO solutions and HAM from mean GRACE/GRACE-FO solution. The values are given in mas

# Internal agreement

## Spatial variability: RMS of differences

2019: initial period of the GRACE-FO mission



*The largest deviations from the average occur for the initial period of the GRACE. For the initial period of the GRACE-FO these variations are definitely lower, however, not as small as for 2006 (best GRACE performance). HAM from JPL is characterized by the best spatial agreement with HAM from the mean GRACE/GRACE-FO. HAM from GFZ is characterized by the biggest spatial differences from the average.*

**Fig. 24.** Maps of RMS of differences between HAM from particular GRACE/GRACE-FO solutions and HAM from mean GRACE/GRACE-FO solution. The values are given in mas

# External validation

## Time series of GAO and GRACE-based HAM

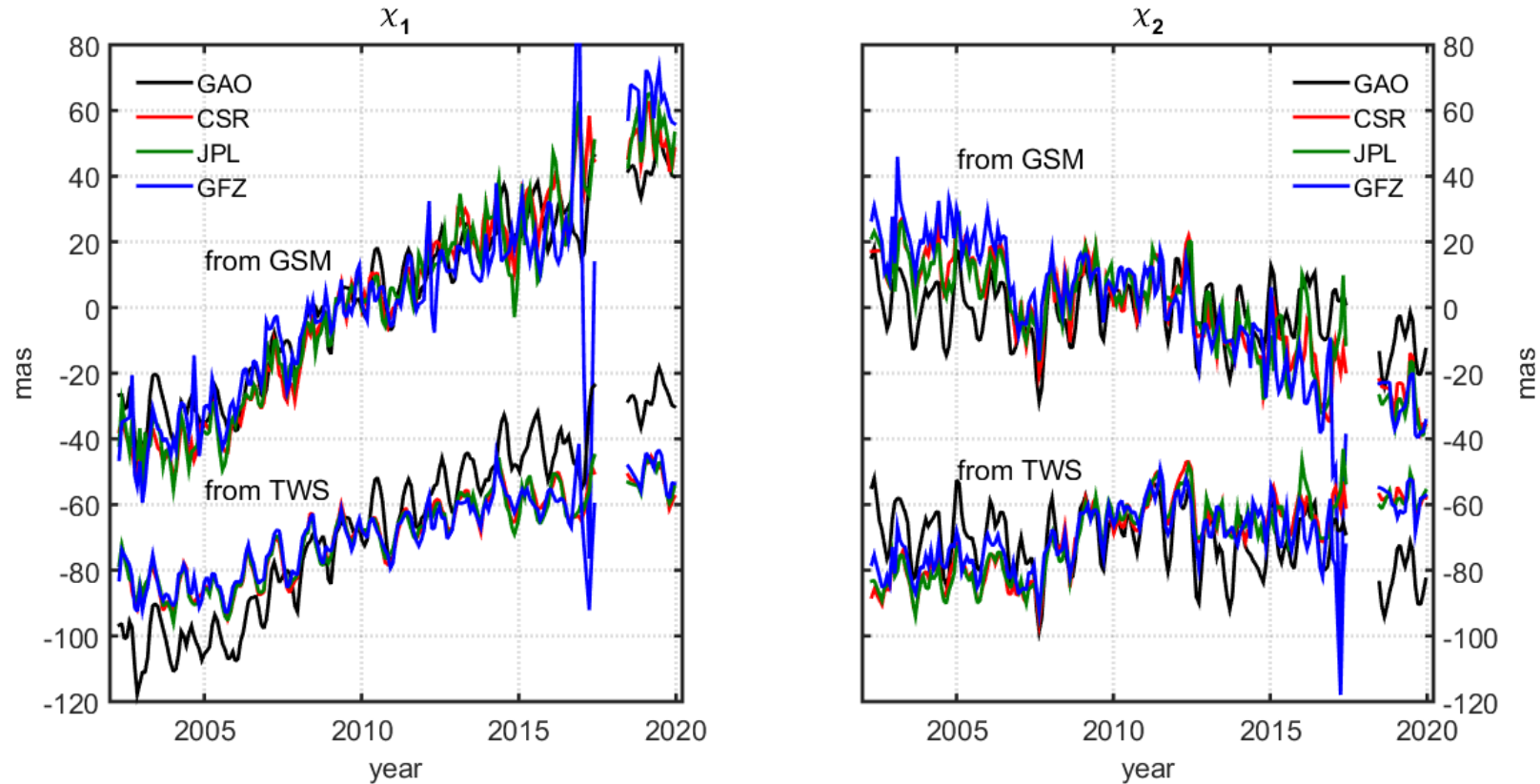


**Fig. 25.** Time series of  $\chi_1$  and  $\chi_2$  components of GAO and HAM computed from GRACE and GRACE-FO monthly solutions: Level-2 data (GSM) and Level-3 data (TWS)

*The trends for GRACE Level-2 data are more consistent with GAO trends, because both types of data have GIA model not removed.*

*The trends for GRACE-FO are difficult to assess due to insufficient data length.*

**Tab. 4.** (a) Standard deviation of GAO and HAM series (in mas), (b) Trends in GAO and HAM series (in mas/year)

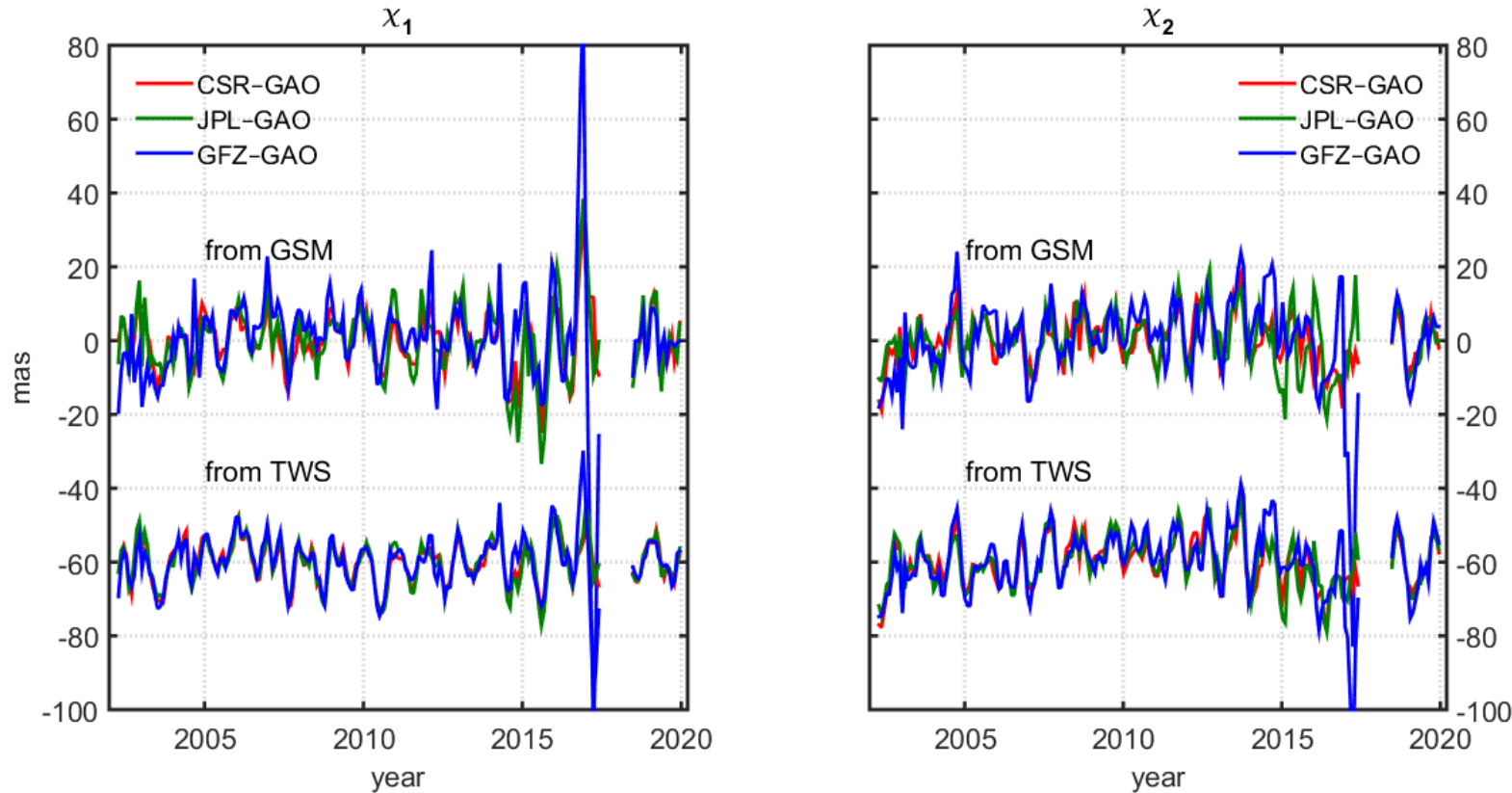
a)		GRACE		GRACE-FO	
		$\chi_1$	$\chi_2$	$\chi_1$	$\chi_2$
	GAO	7.77	9.23	4.32	7.08
CSR	GSM	7.33	8.98	5.62	5.89
JPL	GSM	8.76	9.39	7.07	5.86
GFZ	GSM	15.82	11.86	6.20	5.79
CSR	TWS	5.83	7.51	4.18	3.01
JPL	TWS	5.92	7.45	4.17	2.74
GFZ	TWS	6.60	8.86	4.38	4.25

b)		GRACE		GRACE-FO	
		$\chi_1$	$\chi_2$	$\chi_1$	$\chi_2$
	GAO	5.12	-0.16	3.39	2.80
CSR	GSM	6.38	-2.33	-3.16	-6.33
JPL	GSM	6.05	-2.07	0.15	-3.11
GFZ	GSM	4.67	-3.79	-2.75	-8.25
CSR	TWS	2.40	1.87	-3.48	-0.54
JPL	TWS	2.36	1.91	-1.07	1.90
GFZ	TWS	2.05	0.86	-1.99	-1.91

# External validation

## Differences between GAO and GRACE-based HAM



**Fig. 26.** Differences between HAM obtained from a particular GRACE/GRACE-FO solution and GAO

**Tab. 5.** RMS of differences (root-mean-square errors, RMSE) between HAM from particular GRACE/GRACE-FO solutions and GAO

		GRACE		GRACE-FO	
		$\chi_1$	$\chi_2$	$\chi_1$	$\chi_2$
CSR	GSM	7.70	6.57	5.55	5.05
JPL	GSM	9.64	7.42	7.00	6.01
GFZ	GSM	16.58	12.27	4.50	7.50
CSR	TWS	5.58	6.24	4.16	5.39
JPL	TWS	6.06	6.46	4.19	6.04
GFZ	TWS	7.52	9.17	3.57	7.65

*The GRACE/GRACE-FO Level-3 data provide higher consistency of HAM with GAO than GRACE/GRACE-FO Level-2 data.*

*For GRACE: HAM from TWS CSR is characterized by the smallest errors, HAM from GSM GFZ has the highest errors.*

*For GRACE-FO: the smallest errors are for TWS GFZ ( $\chi_1$ ), and for TWS CSR and GSM CSR ( $\chi_2$ ). The highest errors are for GSM JPL ( $\chi_1$ ) and for TWS GFZ and GSM GFZ ( $\chi_2$ ).*

# External validation

## 19-month periods

It should be kept in mind that:

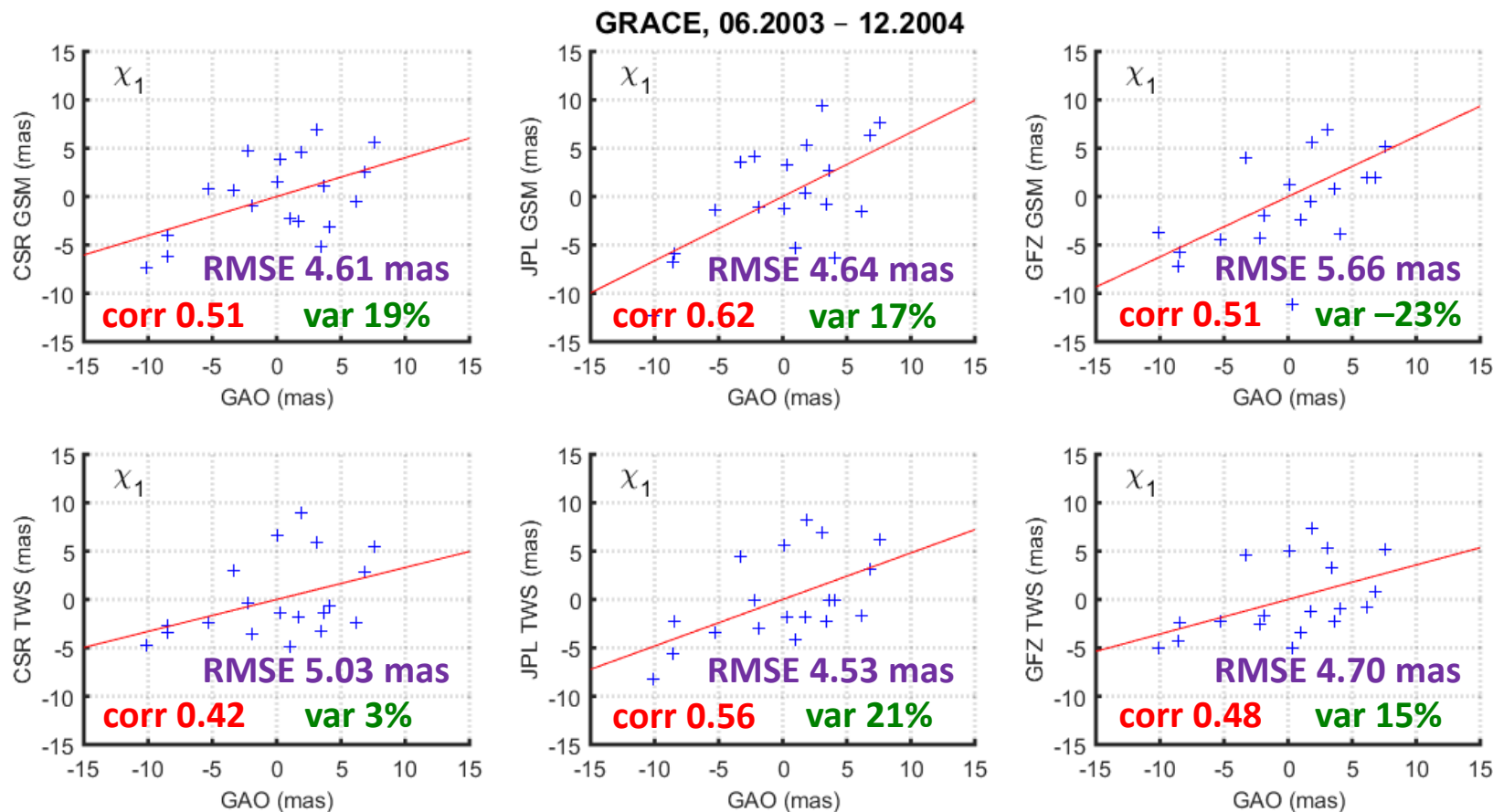
- The considered here time series of GRACE-FO have the length of 19 months only (June 2018 – December 2019);
- Time series for GRACE are available for 163 months (time period April 2002 – June 2017; with occasional gaps);
- Due to different length of data for GRACE and GRACE-FO, the comparison between them may be unreliable;
- Additionally, observations from the initial period of the GRACE-FO mission might be less accurate than observations from later years (e.g. the need for instrument calibration).

Therefore, in order to make GRACE indicates more comparable to those from GRACE-FO, we choose three 19-month periods which are characterized by different accuracy of GRACE measurements:

- June 2003 – December 2004 (initial period of the GRACE mission),
- June 2007 – December 2008 (best GRACE performance),
- June 2015 – December 2016 (terminal phase of the GRACE mission).

# External validation

## 19-month periods



The relative explained variance ( $Var_{exp}$ ) describes the variance agreement between two time series, the first of which is a reference series ( $r$ ) and the second of which is evaluated ( $e$ ):

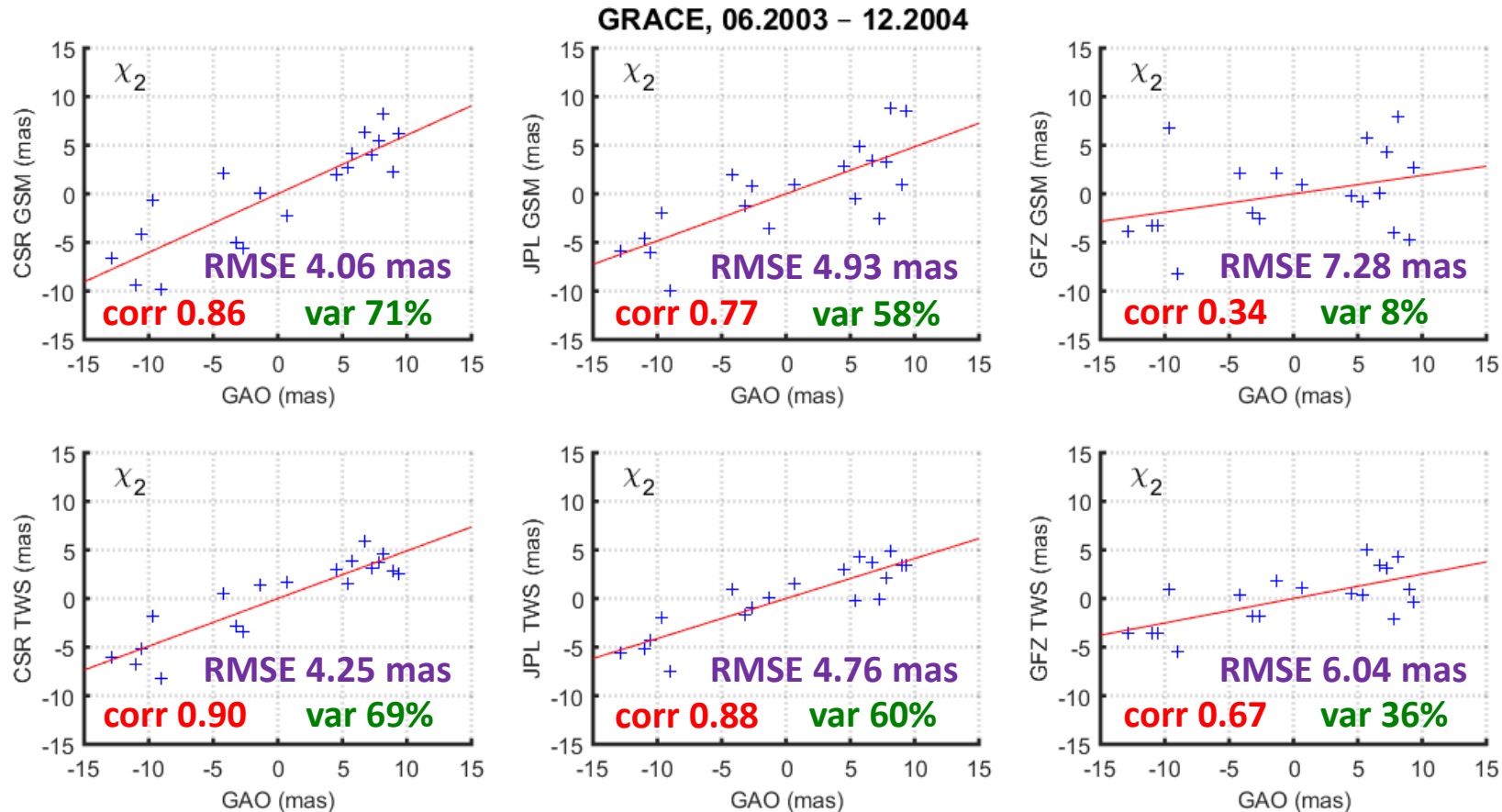
$$Var_{exp} = \left( \frac{Var(r) - Var(r-e)}{Var(r)} \right) \cdot 100\%.$$

The best value for  $Var_{exp}$  is 100%.

**Fig. 27.** Scatter plots showing the relationship between GAO and HAM from particular GRACE/GRACE-FO solutions. The red line was fitted to the data points using the least squares method. The values in purple indicate RMSE, the values in red indicate correlation coefficients between series, the values in green indicate relative explained variances

# External validation

## 19-month periods



**06.2003 – 12.2004:**

For  $\chi_1$ : best JPL TWS and GSM, worst GFZ GSM

For  $\chi_2$ : best CSR TWS and GSM, worst GFZ GSM

Mean RMSE: 4.9 mas ( $\chi_1$ ) and 5.2 mas ( $\chi_2$ )

**Fig. 28.** Scatter plots showing the relationship between GAO and HAM from particular GRACE/GRACE-FO solutions. The red line was fitted to the data points using the least squares method. The values in purple indicate RMSE, the values in red indicate correlation coefficients between series, the values in green indicate relative explained variances

# External validation

## 19-month periods

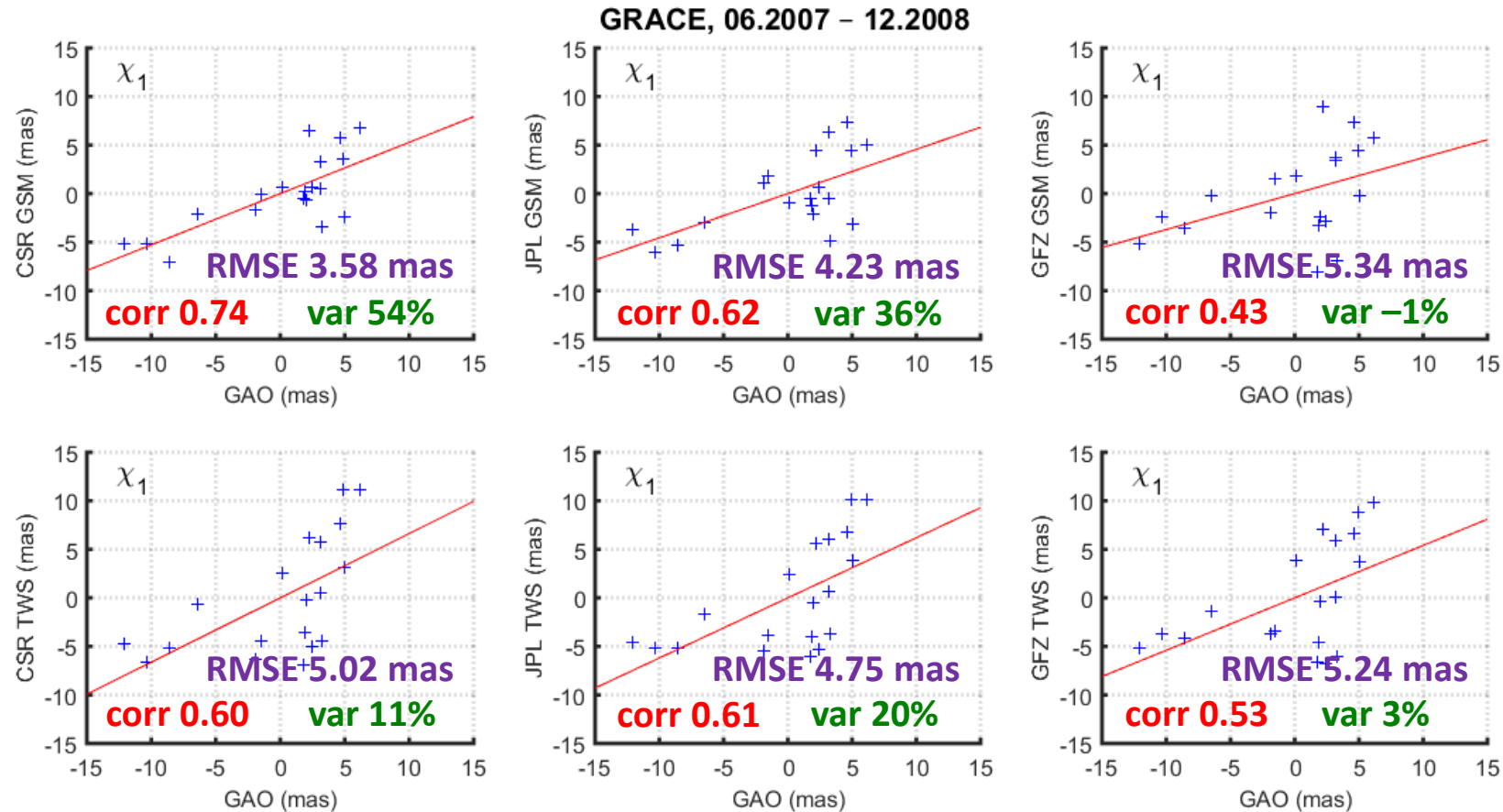
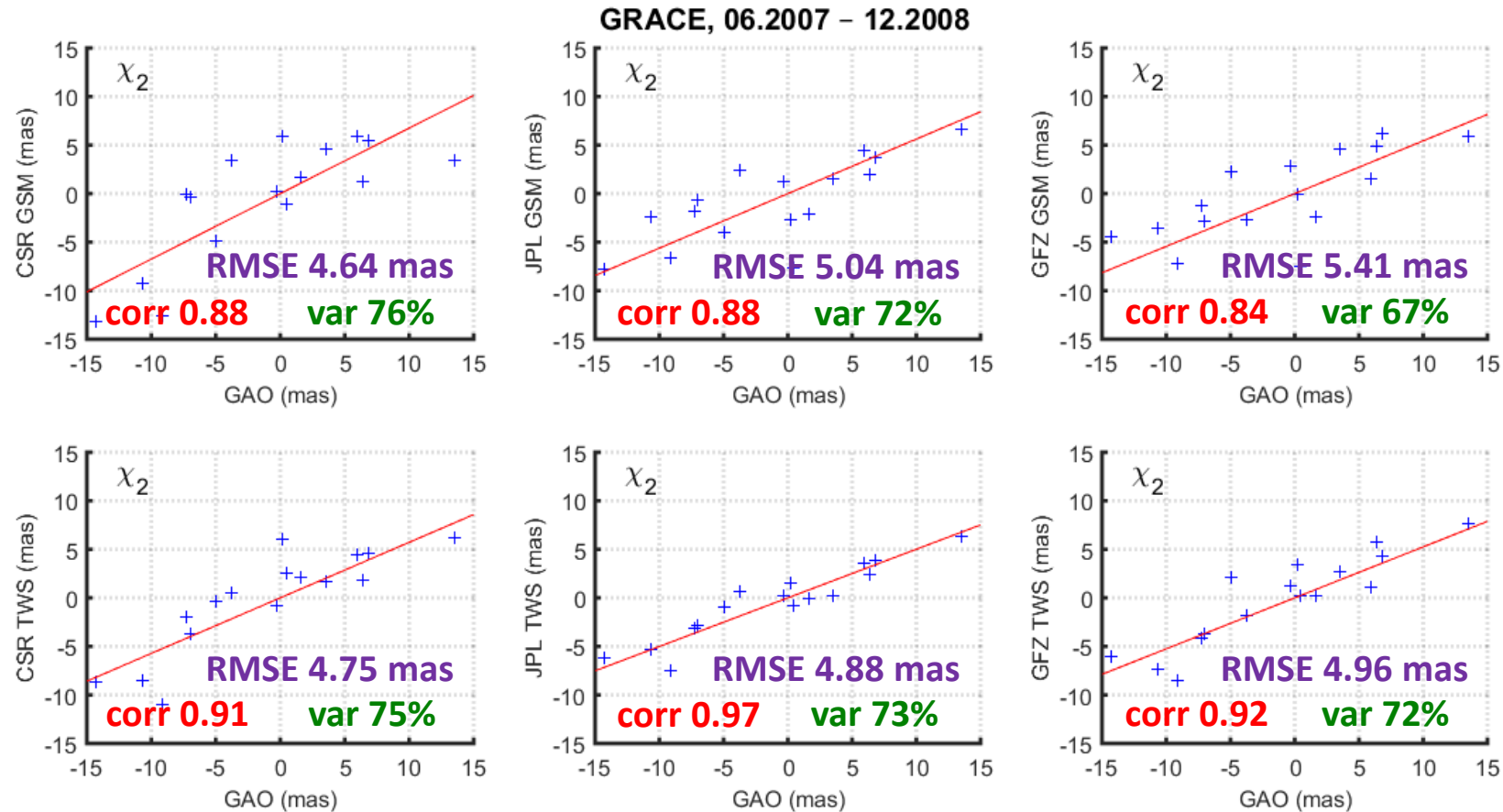


**Fig. 29.** Scatter plots showing the relationship between GAO and HAM from particular GRACE/GRACE-FO solutions. The red line was fitted to the data points using the least squares method. The values in purple indicate RMSE, the values in red indicate correlation coefficients between series, the values in green indicate relative explained variances

# External validation

## 19-month periods



**06.2007 – 12.2008:**

For  $\chi_1$ : best CSR GSM, worst GFZ GSM

For  $\chi_2$ : similar accuracy for all HAM series except HAM from GFZ GSM

Mean RMSE: 4.7 mas ( $\chi_1$ ) and 4.9 mas ( $\chi_2$ )

**Fig. 30.** Scatter plots showing the relationship between GAO and HAM from particular GRACE/GRACE-FO solutions. The red line was fitted to the data points using the least squares method. The values in purple indicate RMSE, the values in red indicate correlation coefficients between series, the values in green indicate relative explained variances

# External validation

## 19-month periods

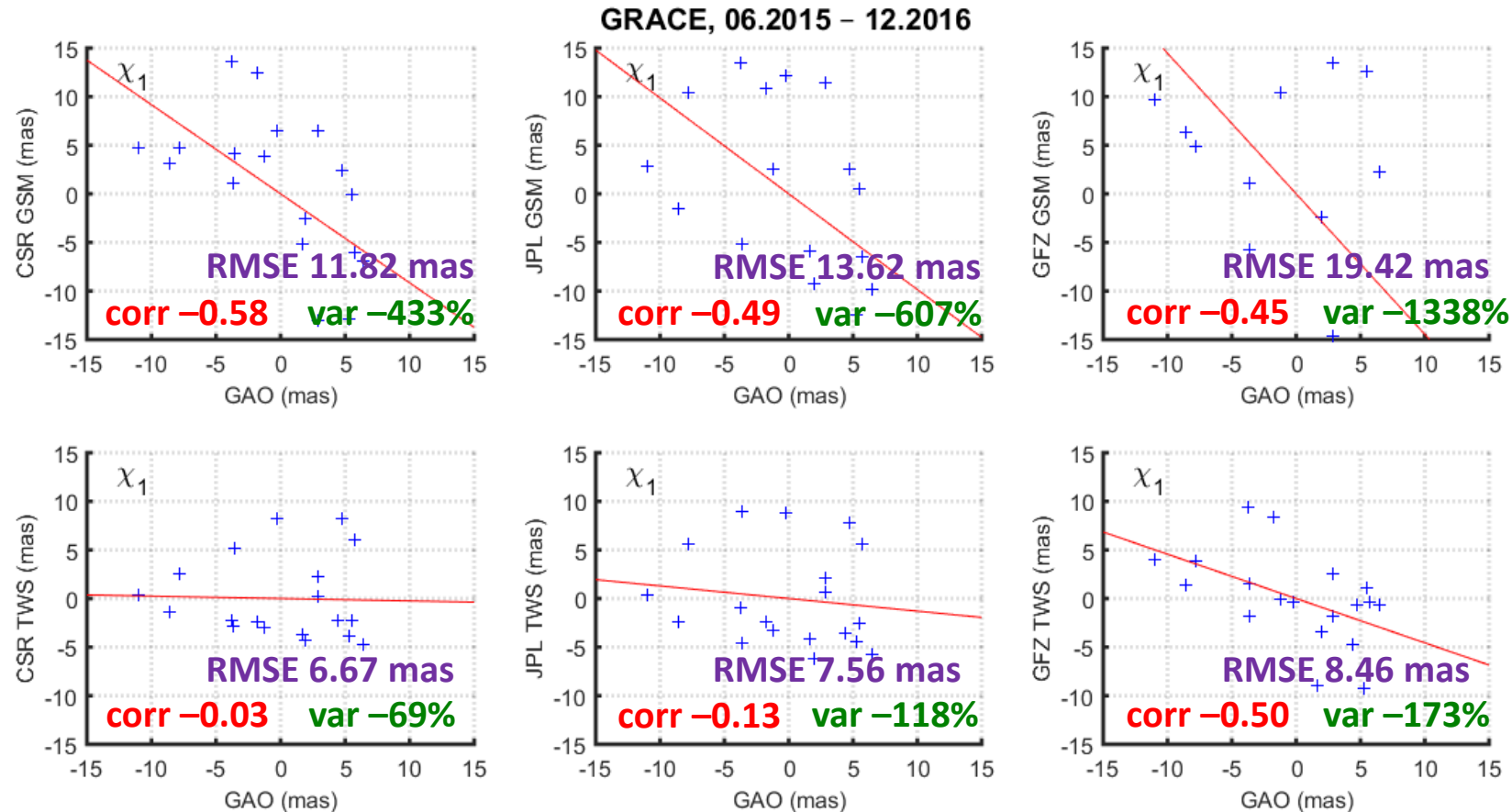
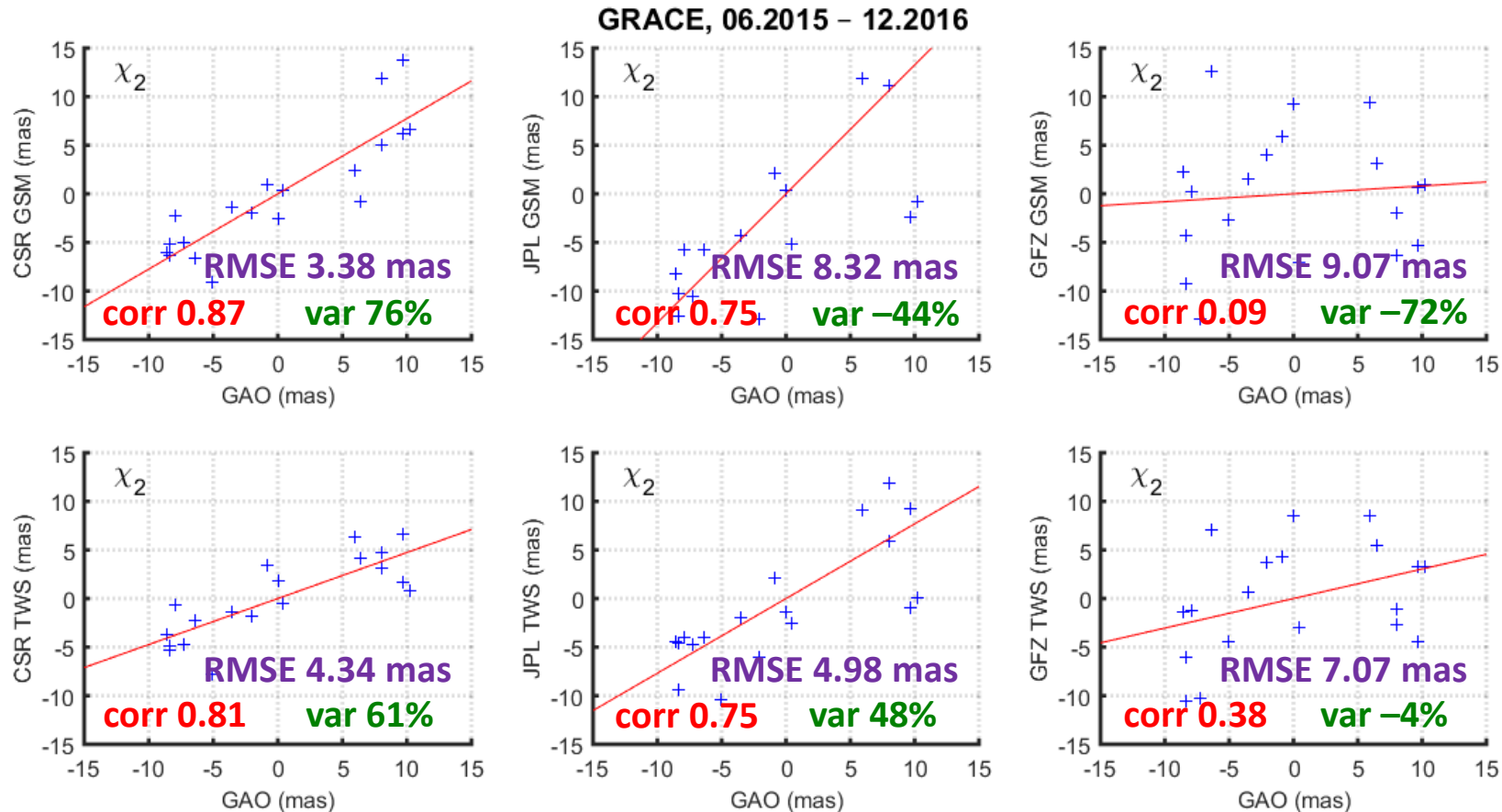


**Fig. 31.** Scatter plots showing the relationship between GAO and HAM from particular GRACE/GRACE-FO solutions. The red line was fitted to the data points using the least squares method. The values in purple indicate RMSE, the values in red indicate correlation coefficients between series, the values in green indicate relative explained variances

# External validation

## 19-month periods



**06.2015 – 12.2016:**

For  $\chi_1$ : best CSR TWS, worst GFZ GSM

For  $\chi_2$ : best CSR TWS and GSM, worst GFZ GSM

Mean RMSE: 11.3 mas ( $\chi_1$ ) and 6.2 mas ( $\chi_2$ )

**Fig. 32.** Scatter plots showing the relationship between GAO and HAM from particular GRACE/GRACE-FO solutions. The red line was fitted to the data points using the least squares method. The values in purple indicate RMSE, the values in red indicate correlation coefficients between series, the values in green indicate relative explained variances

# External validation

## 19-month periods

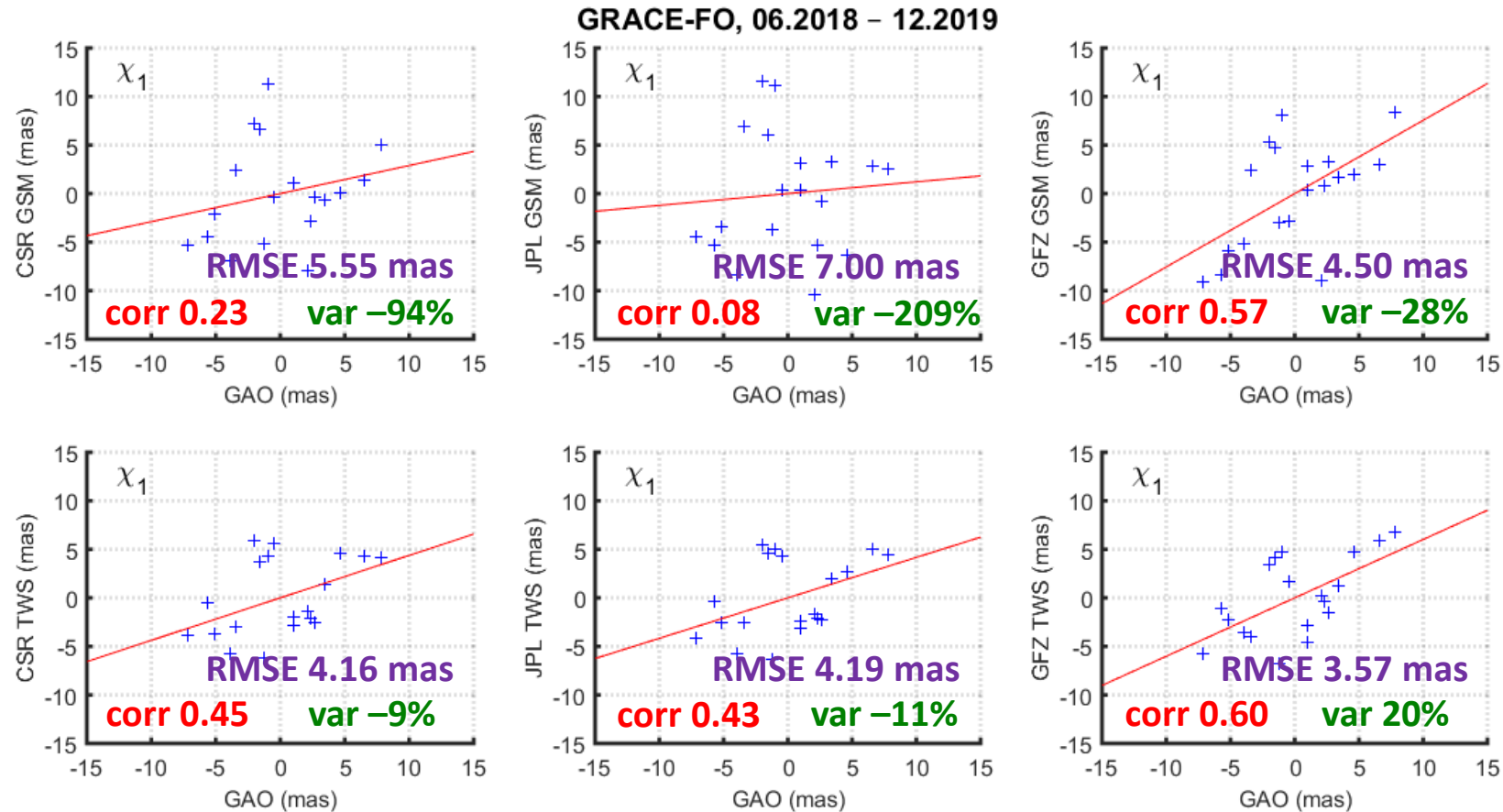
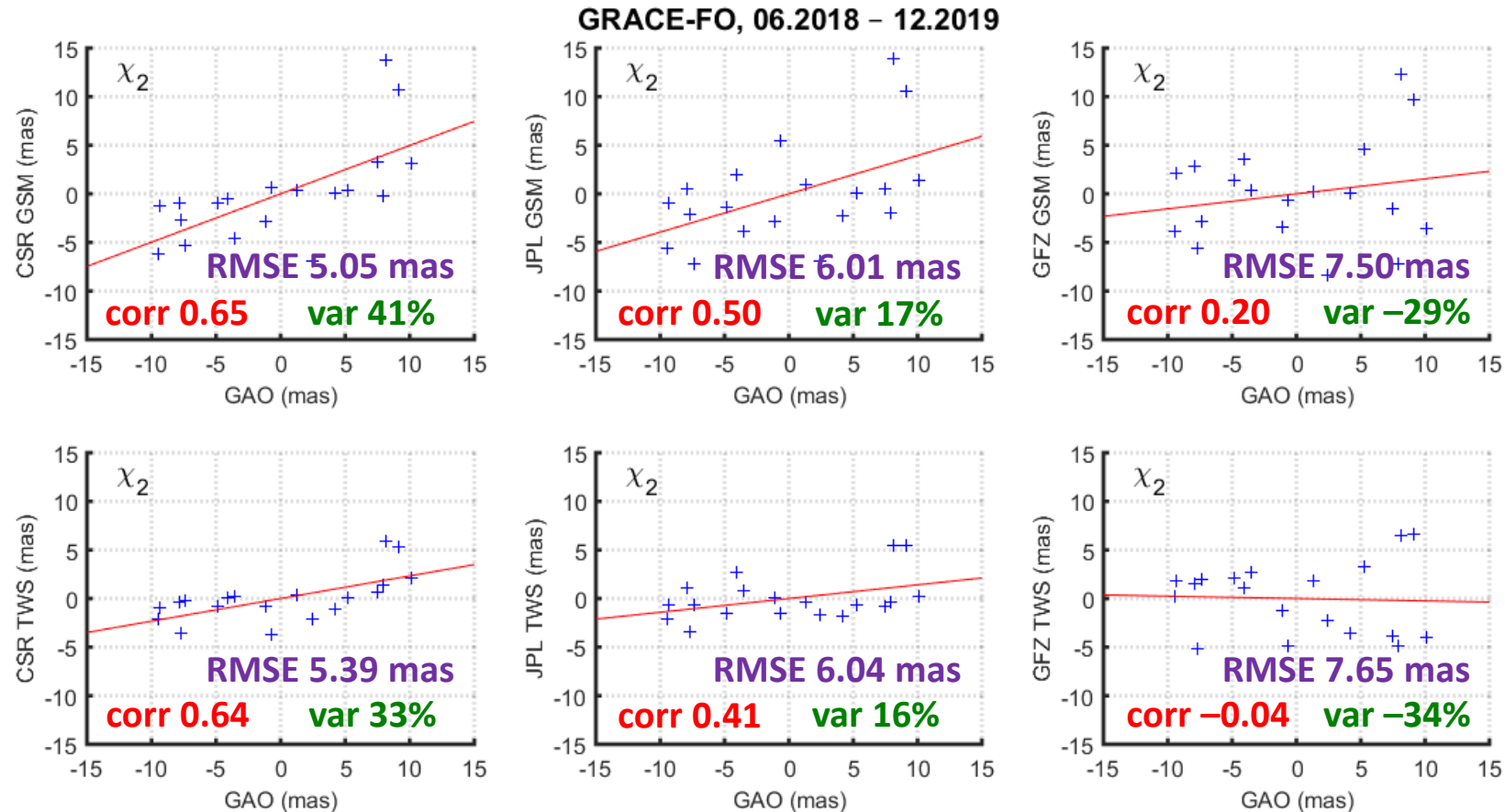


**Fig. 33.** Scatter plots showing the relationship between GAO and HAM from particular GRACE/GRACE-FO solutions. The red line was fitted to the data points using the least squares method. The values in purple indicate RMSE, the values in red indicate correlation coefficients between series, the values in green indicate relative explained variances

# External validation

## 19-month periods



**06.2018 – 12.2019:**  
 For  $\chi_1$ : best GFZ TWS, worst JPL GSM  
 For  $\chi_2$ : best CSR TWS and GSM, worst GFZ GSM and TWS  
 Mean RMSE: 4.8 mas ( $\chi_1$ ) and 6.3 mas ( $\chi_2$ )

**Fig. 34.** Scatter plots showing the relationship between GAO and HAM from particular GRACE/GRACE-FO solutions. The red line was fitted to the data points using the least squares method. The values in purple indicate RMSE, the values in red indicate correlation coefficients between series, the values in green indicate relative explained variances

# Comparison between HAM from GSM, TWS, and MAS

## Time series of GAO and GRACE-based HAM

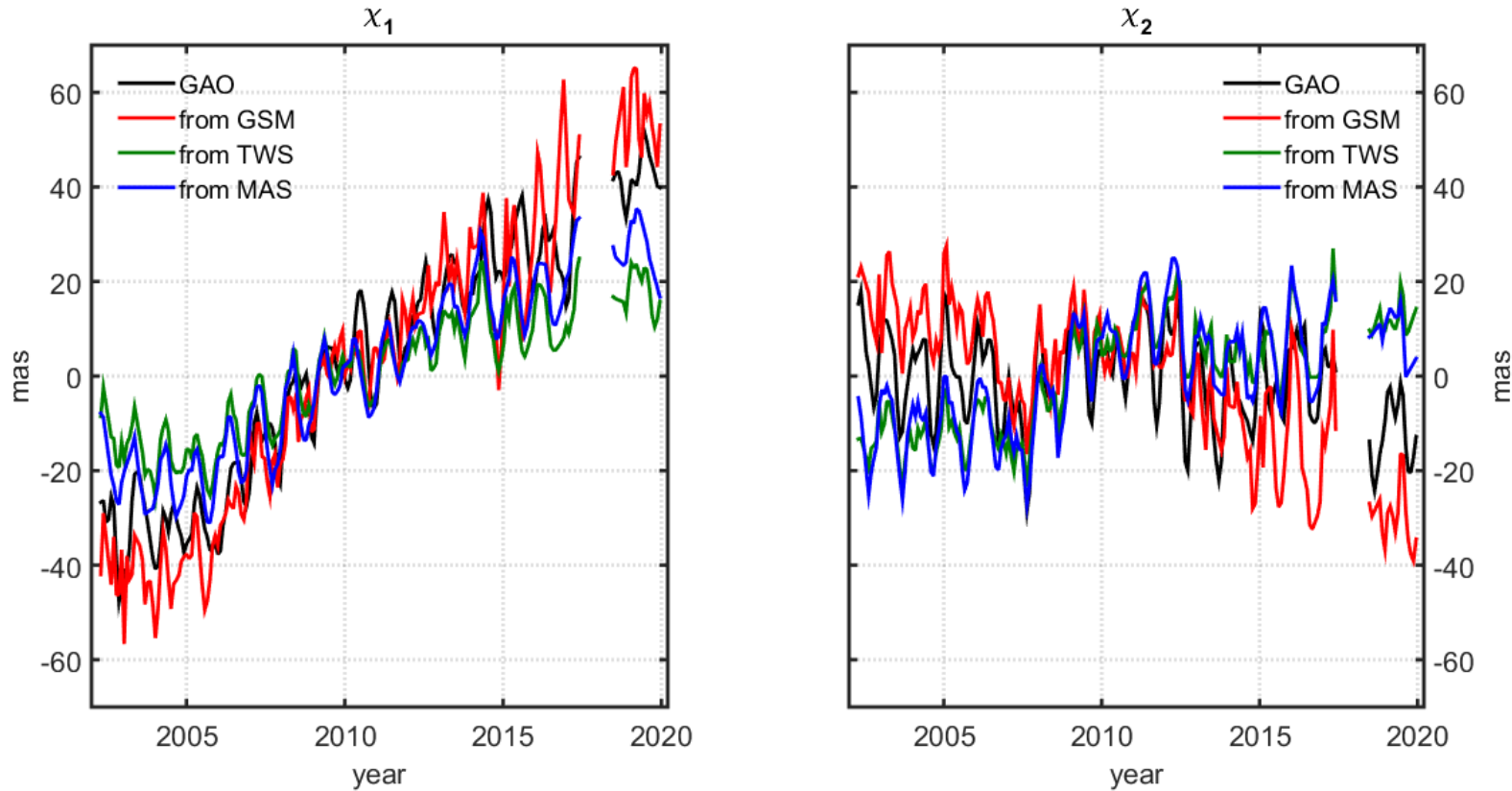


**Fig. 35.** Time series of  $\chi_1$  and  $\chi_2$  components of GAO and HAM computed from different types of GRACE and GRACE-FO data (GSM, TWS, MAS). All GRACE-based HAM series were computed using data from JPL

**Tab. 6.** (a) Standard deviation of GAO and HAM series (in mas), (b) Trends in GAO and HAM series (in mas/year)

a)		GRACE		GRACE-FO	
		$\chi_1$	$\chi_2$	$\chi_1$	$\chi_2$
GAO		7.77	9.23	4.32	7.08
JPL	GSM	8.76	9.39	7.07	5.86
JPL	TWS	5.92	7.45	4.17	2.74
JPL	MAS	6.82	9.22	5.21	4.23

b)		GRACE		GRACE-FO	
		$\chi_1$	$\chi_2$	$\chi_1$	$\chi_2$
GAO		5.12	-0.16	3.39	2.80
JPL	GSM	6.05	-2.07	0.15	-3.11
JPL	TWS	2.36	1.91	-1.07	1.90
JPL	MAS	3.48	1.78	-3.17	-4.91

*The trends for GRACE Level-2 data are more consistent with GAO trends, because both types of data have GIA model not removed.*

*HAM from TWS and from MAS have similar trends and STD of series.*

# Comparison between HAM from GSM, TWS, and MAS

## Differences between GAO and GRACE-based HAM

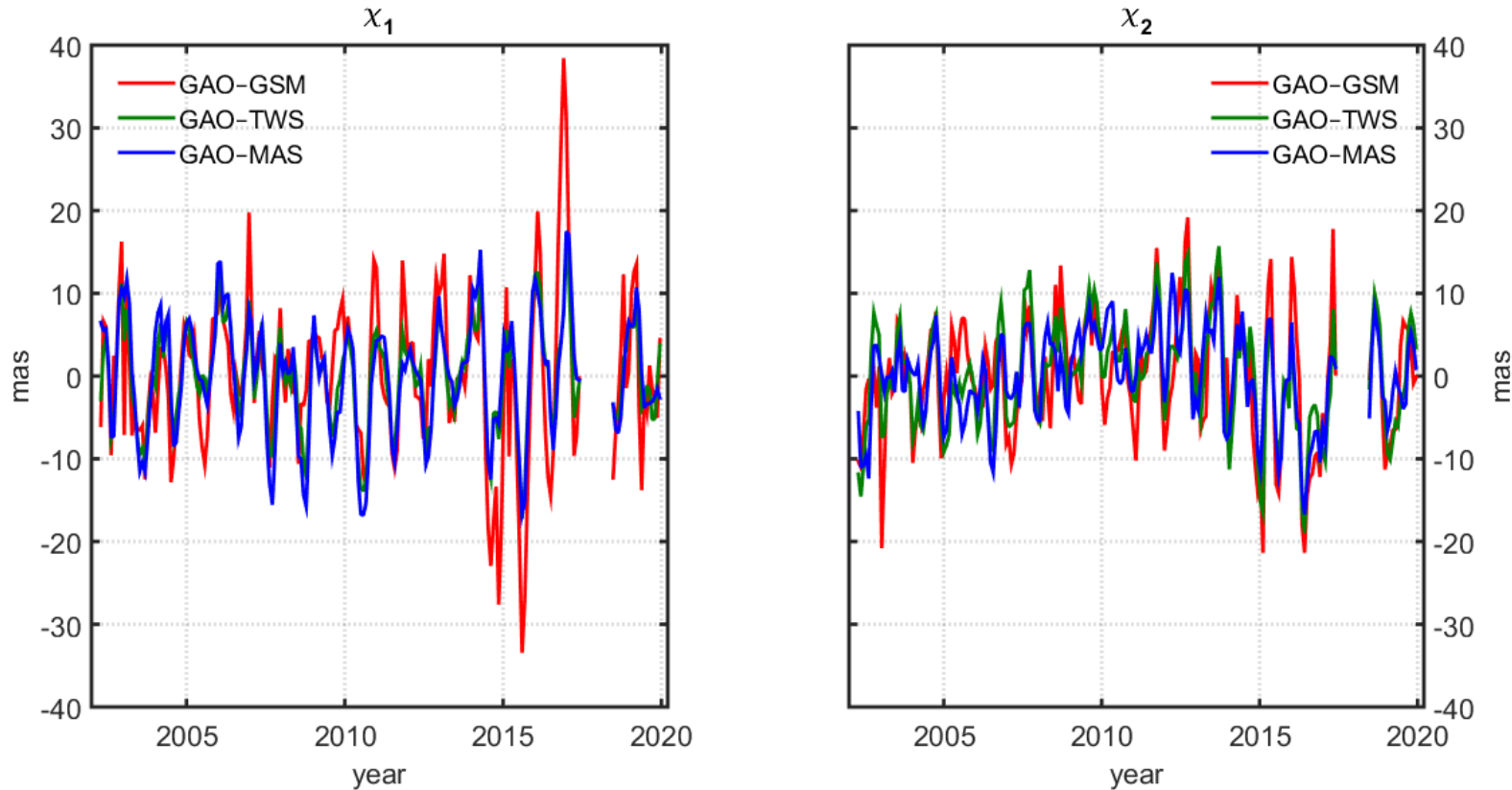


**Fig. 36.** Differences between HAM obtained from a particular GRACE/GRACE-FO solution (JPL GSM, JPL TWS, JPL MAS) and GAO

**Tab. 7.** RMS of differences (root-mean-square errors, RMSE) between HAM from particular GRACE/GRACE-FO solutions (JPL GSM, JPL TWS, JPL MAS) and GAO

		GRACE		GRACE-FO	
		$\chi_1$	$\chi_2$	$\chi_1$	$\chi_2$
JPL	GSM	9.64	7.42	7.00	6.01
JPL	TWS	6.06	6.46	4.19	6.04
JPL	MAS	7.18	5.66	4.98	3.92

*The GRACE/GRACE-FO Level-3 data provide the lowest errors of HAM: TWS is better for  $\chi_1$  while MAS works better for  $\chi_2$ . It should be kept in mind that  $\chi_2$  is more sensitive to mass changes over continents, so it can be concluded that mascons are the most appropriate to analyze water storage changes on lands (and resulting PM excitation).*

*The GRACE/GRACE-FO Level-2 data provide the lowest consistency of HAM with GAO.*

# Comparison between HAM from GSM, TWS, and MAS

## Scatter plots, RMSE, correlation coefficients, relative explained variance

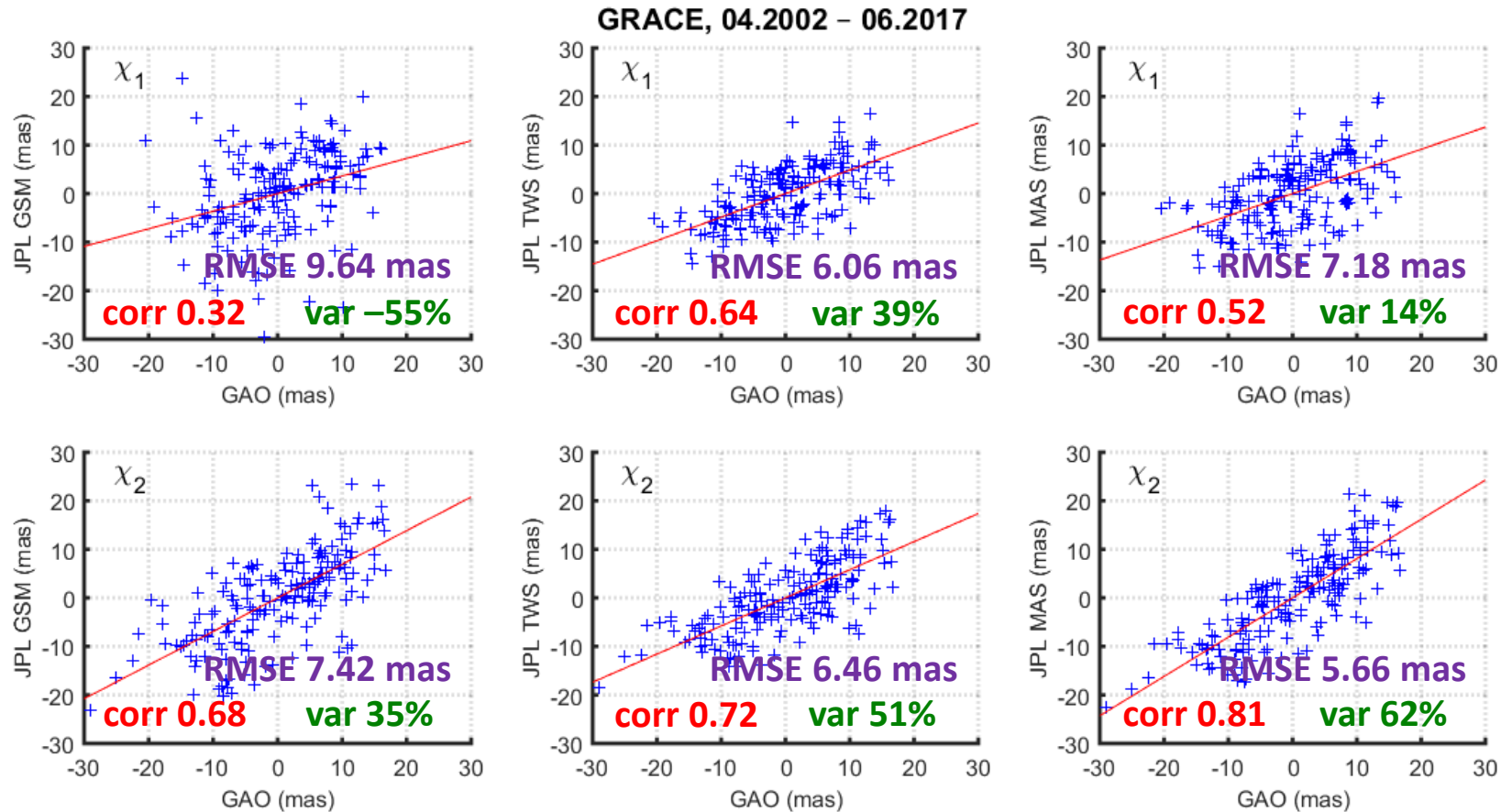
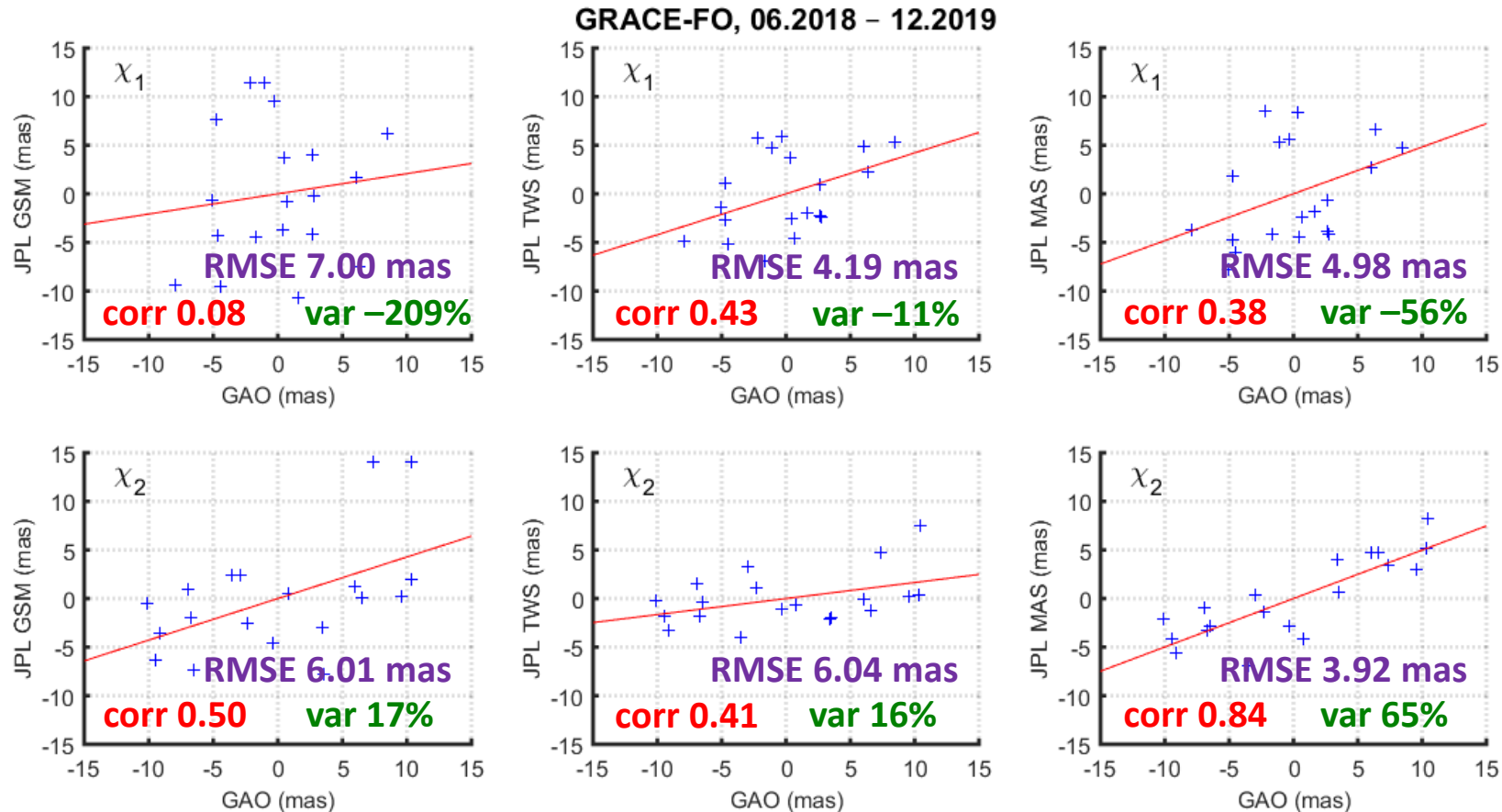


**Fig. 37.** Scatter plots showing the relationship between GAO and HAM from different types of GRACE/GRACE-FO data (GSM, TWS, MAS). The red line was fitted to the data points using the least squares method. The values in purple indicate RMSE, the values in red indicate correlation coefficients between series, the values in green indicate relative explained variances

# Comparison between HAM from GSM, TWS, and MAS

Scatter plots, RMSE, correlation coefficients, relative explained variance



Scatter plots, RMSE, correlation coefficients and relative explained variances prove the highest consistency between GAO and HAM from TWS for  $\chi_1$ , and between GAO and HAM from MAS for  $\chi_2$ .

**Fig. 38.** Scatter plots showing the relationship between GAO and HAM from different types of GRACE/GRACE-FO data (GSM, TWS, MAS). The red line was fitted to the data points using the least squares method. The values in purple indicate RMSE, the values in red indicate correlation coefficients between series, the values in green indicate relative explained variances

# Conclusions

## Internal agreement:

- The highest internal agreement between different GRACE and GRACE-FO solutions can be obtained when comparing data from CSR and JPL. The GRACE and GRACE-FO series from GFZ deviate the most from the average and from other solutions.
- Spatial variability of HAM is similar for all GRACE and GRACE-FO data. The largest deviations from the average occur for the initial period of the GRACE. For the initial period of the GRACE-FO these variations are definitely lower, however, not as small as for 2006 (best GRACE performance).
- The highest agreement between different GRACE/GRACE-FO-based HAM is obtained when GRACE/GRACE-FO Level-3 data are used.
- HAM from particular GRACE/GRACE-FO solutions are more compatible with each other for  $\chi_2$  than for  $\chi_1$ .

## External validation:

- The highest agreement between GRACE/GRACE-FO-based HAM and GAO is obtained when GRACE/GRACE-FO Level-3 data are used.
- GRACE Level-2 data are the most appropriate for trend analysis, however, trends for GRACE-FO are difficult to assess due to insufficient data length.

# Conclusions

- The analysis of first 19 months of GRACE-FO data showed that the accuracy of GRACE-FO-based HAM is rather similar to the accuracy of GRACE-based HAM in its initial period of the GRACE mission, worse than the accuracy of GRACE-based HAM in its best period and higher than the accuracy of GRACE-based HAM in the terminal phase of the GRACE mission.
- Compared to the GRACE mission, the GRACE-FO has increased the accuracy of determining especially the  $\chi_1$  component of HAM.
- In general, the current accuracy of HAM from GRACE Follow-On mission (RMSE: 4.8 mas for  $\chi_1$  and 6.3 mas for  $\chi_2$ ) meets expectations. In the following months, after full calibration of the instruments, this accuracy is expected to increase.

## **HAM from GSM vs HAM from TWS vs HAM from MAS:**

- There is a high dependence between HAM from TWS data and HAM from MAS data, and a poor consistency between HAM from GSM and HAM from MAS.
- The GRACE/GRACE-FO Level-3 data provide the lowest errors of HAM: TWS is better for  $\chi_1$  while MAS works better for  $\chi_2$ .

# References

- Eubanks, T. M. (1993). Variations in the orientation of the Earth. Contributions of Space Geodesy to Geodynamics: Earth Dynamics, Vol 24 Geodynamics Series, pp. 1–54, Eds Smith, D.E. and Turcotte, D.L, AGU, Washington
- Gross, R. (2015). Theory of earth rotation variations. In VIII Hotine-Marussi Symposium on Mathematical Geodesy, Sneeuw, N., Novák, P., Crespi, M., Sansò, F., Eds., Springer: Cham, Switzerland, 2015, p. 142
- Śliwińska, J., Nastula, J., Dobslaw, H., Dill, R. (2020). Evaluating Gravimetric Polar Motion Excitation Estimates from the RL06 GRACE Monthly-Mean Gravity Field Models. Remote Sens., 12, 930
- Watkins, M.M., Wiese, D.N., Dah-Ning, Y., Boening, C., Landerer, F.W. (2015). Improved methods for observing Earth's time variable mass distribution with GRACE using spherical cap mascons, J. Geophys. Res. Solid Earth, 120, 2648-2671, doi:10.1002/2014JB011547
- Wiese, D., Landerer, F.W., Watkins, M.M. (2016). Quantifying and reducing leakage errors in the JPL RL05M GRACE mascon solution. Water Resour. Res., 52, 7490-7502, doi: 10.1002/2016WR019344

# List of acronyms

AAM – atmospheric angular momentum  
AOD1B – Atmosphere and Ocean De-Aliasing Level-1B  
CSR – Center for Space Research  
EAM – effective angular momentum  
ECMWF – European Centre for Medium-Range Weather Forecasts  
EOP – Earth orientation parameters  
FWHM – full width at half maximum  
GAM – geodetic angular momentum  
GAO – geodetic residuals: GAM–AAM–OAM  
GFO (or GRACE-FO) – Gravity Recovery and Climate Experiment Follow-On  
GFZ – GeoForschungsZentrum  
GIA – glacial isostatic adjustment  
GNSS – global navigation satellite system  
GRACE – Gravity Recovery and Climate Experiment  
GSM – GRACE satellite-only model  
HAM – hydrological angular momentum  
IERS – International Earth Rotation and Reference System Service

ITRF – International Terrestrial Reference Frame  
JPL – Jet Propulsion Laboratory  
LOD – length-of-day  
LSDM – Land Surface Discharge Model  
HAM – hydrological angular momentum  
IERS – International Earth Rotation and Reference System Service  
ITRF – International Terrestrial Reference Frame  
JPL – Jet Propulsion Laboratory  
LOD – length-of-day  
LSDM – Land Surface Discharge Model  
MAS – mascon  
MPIOM – Max Planck Institute Ocean Model  
OAM – oceanic angular momentum  
PM – polar motion  
RMS – root mean square  
RMSE – root mean square error  
SLR – satellite laser ranging  
STD – standard deviation  
TWS – terrestrial water storage  
VLBI – very long baseline interferometry

# Acknowledgement

This research was funded by National Science Center, Poland (NCN), grant number 2018/31/N/ST10/00209, and by the Polish National Agency for Academic Exchange (NAWA) grant number PPI/APM/2018/1/00032/U/001.



# Thank you



Warsaw University  
of Technology

# Preliminary hydrological polar motion excitation estimates from the GRACE Follow-On mission

Justyna Śliwińska<sup>1</sup>, Małgorzata Wińska<sup>2</sup>, Jolanta Nastula<sup>1</sup>

<sup>1</sup>Space Research Centre, Polish Academy of Sciences, Warsaw, Poland

<sup>2</sup>Institute of Roads and Bridges, Warsaw University of Technology, Warsaw, Poland



To derive equation shown in slide 20, we used the equations and parameters shown in (Gross, R. Theory of Earth Rotation Variations), but we made some additional computations to obtain a final equation. Below you can find the steps of deriving Equation shown on slide 20. The full information needed to derive the equations can be found in (Eubanks, 1993) and (Gross 2015, Chapter 3.09.2.1 and 3.09.5).

Eubanks, T.M. Variations in the orientation of the Earth. In Contributions of Space Geodesy to Geodynamics: Earth Dynamics: Geodynamic Series; Smith, D.E., Turcotte, D.L., Eds.; American Geophysical Union: Washington, DC, USA, 1993; Volume 24, pp. 1–54.

Gross, R. Theory of earth rotation variations. In VIII Hotine-Marussi Symposium on Mathematical Geodesy; Sneeuw, N., Novák, P., Crespi, M., Sansò, F., Eds.; Springer: Cham, Switzerland, 2015; p. 142.

According Gross (2015)

Earth Rotation Variations - Long Period in Treatise on Geophysics

*Parameters*

$$\Omega = 7.292115 \times 10^{-5} \text{ rads}^{-1}$$

$$C = 8.0365 \times 10^{37} \text{ kgm}^2$$

$$B = 8.0103 \times 10^{37} \text{ kgm}^2$$

$$A = 8.0101 \times 10^{37} \text{ kgm}^2$$

$$A_c = 9.1168 \times 10^{36} \text{ kgm}^2$$

$$\varepsilon_c = 2.546 \times 10^{-3}$$

$$\sigma_o = 1 * 2\pi / 434.2 / 24. / 3600$$

$$A'_m = A' - A_c$$

$$A' = (B - A) / 2$$

-----

$$\chi_x = \frac{h_x(t) + \Omega \left[ 1 + (k'_2 + \text{real}\Delta k'_{an}) \right] \Delta I_{xz}(t)}{\left[ C - A' + A'_m + \varepsilon_c A_c \right] \sigma_o} \quad (41)$$

$$k'_2 = -0.305$$

$$\text{real}\Delta k'_{an} = -0.011$$

$$1 + k'_2 - \text{real}\Delta k'_{an} = 1 - 0.305 - 0.011 = 1 - 0.316 = 0.684$$

$$\chi_x = \frac{h_x(t) + 0.684\Omega \Delta I_{xz}(t)}{\left[ C - A' + A'_m + \varepsilon_c A_c \right] \sigma_o} \quad (41)$$

$$A'_m = A' - A_c$$

↓

$$\chi_x = \frac{h_x(t) + 0.684\Omega \Delta I_{xz}(t)}{\left[ C - A' + A' - A_c + \varepsilon_c A_c \right] \sigma_o}$$

$$\chi_x = \frac{h_x(t) + 0.684\Omega \Delta I_{xz}(t)}{\left[ C + A_c (\varepsilon_c - 1) \right] \sigma_o}$$

$$\chi_x = \frac{h_x(t) + 0.684\Omega \Delta I_{xz}(t)}{\left[ C + A_c (\varepsilon_c - 1) \right] \sigma_o} \frac{\left[ C - A' \right] \Omega}{\left[ C - A' \right] \Omega}$$

$$[C + A_c (\varepsilon_c - 1)] \sigma_o = 1.1931E + 37$$

$$[C - A'] \Omega = 1.9178E + 37$$

$$\frac{[C - A'] \Omega}{[C + A_c (\varepsilon_c - 1)] \sigma_o} \approx 1.608$$

↓

$$\chi_x = \frac{1.608 [h_x(t) + 0.684 \Omega \Delta I_{xz}(t)]}{[C - A'] \Omega} \quad (44)$$

similarly

$$\chi_y = \frac{1.608 [h_y(t) + 0.684 \Omega \Delta I_{yz}(t)]}{[C - A'] \Omega} \quad (45)$$

After setting the relive angular momenta terms  $h_x(t), h_y(t)$  to zero

$$\chi_x = \frac{1.608 * 0.684 \Delta I_{xz}(t)}{[C - A']}$$

similarly

$$\chi_y = \frac{1.608 * 0.684 \Delta I_{yz}(t)}{[C - A']}$$

Now coming to the reation between time dependent changes in the degree-2 Stokes coefficients and the relevant elements of the inertia tensor of the load

$$\Delta C_{21}(t) + \Delta S_{21}(t) = -(1 - k'_2 + \Delta k'_{an}) \frac{\sqrt{3/5}}{Ma^2} (\Delta I_{xz}^L + i \Delta I_{yz}^L) \quad (87)$$

L indicates that the quantity is just for the load

$$\Delta C_{21}(t) + \Delta S_{21}(t) = -0.684 \frac{\sqrt{3/5}}{Ma^2} (\Delta I_{xz}^L + i \Delta I_{yz}^L)$$

Now substituting formulas for  $\chi_x, \chi_y$

$$\Delta C_{21}(t) + \Delta S_{21}(t) = -0.684 \frac{\sqrt{3/5}}{Ma^2} \frac{C - A'}{1.608 * 0.684} (\chi_x(t) + i \chi_y(t)) \quad (89)$$